Early anteroposterior regionalisation of human neural crest is shaped by a pro-mesodermal factor

Early anteroposterior regionalisation of human neural crest is shaped by a pro-mesodermal factor

Antigoni Gogolou[1,2], Celine Souilhol[1,2], Ilaria Granata[3], Filip J Wymeersch[4], Ichcha Manipur[3], Matthew Wind[1,2], Thomas JR Frith[1,2], Maria Guarini[5], Alessandro Bertero[6], Christoph Bock[5,7], Florian Halbritter[8], Minoru Takasato[4, 9], Mario R Guarracino[10], Anestis Tsakiridis[1,2*]

[1]Centre for Stem Cell Biology, Department of Biomedical Science, The University of Sheffield, Western Bank, Sheffield S10 2TN United Kingdom.

[2]Neuroscience Institute, The University of Sheffield, Western Bank, Sheffield, S10 2TN United Kingdom.

[3]Computational and Data Science Laboratory, High Performance Computing and Networking Institute, National Research Council of Italy, Napoli, Italy.

[4]Laboratory for Human Organogenesis, RIKEN Center for Biosystems Dynamics Research, 2-2-3 Minatojima-minamimachi, Chuo-ku, Kobe, 650-0047, Japan.

[5]CeMM Research Center for Molecular Medicine of the Austrian Academy of Sciences, Vienna, Austria.

[6] Molecular Biotechnology Center, Department of Molecular Biotechnology and Health Sciences, University of Torino, 10126 Torino, Italy.

[7]Institute of Artificial Intelligence, Center for Medical Statistics, Informatics, and Intelligent Systems, Medical University of Vienna, Vienna, Austria.

[8]St. Anna Children´s Cancer Research Institute (CCRI), Vienna, Austria.

[9]Laboratory of Molecular Cell Biology and Development, Department of Animal Development and Physiology, Graduate School of Bio-studies, Kyoto University, Kyoto, 606-8501, Japan

[10]University of Cassino and Southern Lazio, Cassino, Italy.

*corresponding author: a.tsakiridis@sheffield.ac.uk

Running title: Trunk neural crest and axial progenitors

Keywords: Axial identity/Brachyury/Hox/Neuromesodermal progenitors/Neural crest

Abstract

The neural crest (NC) is an important multipotent embryonic cell population and its impaired specification leads to various developmental defects, often in an anteroposterior (A-P) axial level-specific manner. The mechanisms underlying the correct A-P regionalisation of human NC cells remain elusive. Recent studies have indicated that trunk NC cells, the presumed precursors of the childhood tumour neuroblastoma, are derived from neuromesodermal-potent progenitors of the postcranial body (NMPs). Here we employ human embryonic stem cell differentiation to define how NMP-derived NC cells acquire a posterior axial identity. We

show that TBXT, a pro-mesodermal transcription factor, mediates early posterior NC regionalisation together with WNT signalling effectors. This occurs by TBXT-driven chromatin remodelling via its binding in key enhancers within HOX gene clusters and other posterior regulator-associated loci. In contrast, posteriorisation of NMP-derived spinal cord cells is TBXT/WNT-independent and takes place under the influence of FGF signalling. Our work reveals a previously unknown role of TBXT in influencing posterior NC fate and points to the existence of temporally discrete, cell type-dependent modes of posterior axial identity control.

Introduction

The neural crest (NC) is a multipotent cell population, which arises in the dorsal neural plate/non-neural ectoderm border region during vertebrate embryogenesis and generates a variety of cell types following epithelial-to-mesenchymal transition and migration through diverse routes. NC cells emerge at all levels of the anteroposterior (A-P) axis and their A-P position determines the identity of their derivatives: cranial NC produces mesoectodermal cell types (e.g. dermis, cartilage, bone), melanocytes, neurons and glia colonizing the head; vagal NC cells, arising between somites 1–7, contribute (together with their sacral counterparts emerging at axial levels posterior to somite 28) predominantly to the enteric nervous system and includes a subpopulation (cardiac NC) that generates various heart structures; trunk NC generates dorsal root/sympathetic neurons, adrenal chromaffin cells and melanocytes (reviewed in (Le Douarin et al., 2004, Rocha et al., 2020, Rothstein et al., 2018). Defects in the specification, differentiation or migration of NC cells lead to a wide spectrum of serious developmental disorders, often in an axial level-specific manner and are known collectively as neurocristopathies (Pilon, 2021, Vega-Lopez et al., 2018). The use of human pluripotent stem cell (hPSC) differentiation offers an attractive platform for the study of human NC biology and neurocristopathies as well as an indefinite *in vitro* source of clinically relevant NC-associated cell populations for regenerative medicine applications. However, the cellular and molecular mechanisms directing the acquisition of distinct A-P axial identities by human NC cells remain largely undefined. In turn, this obviates the design of optimised hPSC differentiation protocols aiming to produce NC derivatives as well as the dissection of the links between human neurocristopathy emergence and the axial identity of the NC cells affected.

In vivo, the A-P patterning of the vertebrate embryonic body and its nascent cellular components relies on the coordinated action of Hox gene family members (arranged as paralogous groups (PG) in four distinct chromosomal clusters: A, B, C and D). In mammals, transcriptional activation of Hox genes is initiated during gastrulation, within the posterior part of the embryo around the primitive streak and proceeds in a sequential manner

reflecting their 3'-to-5' genomic order, a phenomenon described as temporal collinearity or the Hox clock (Deschamps & Duboule, 2017, Dolle et al., 1989, Izpisua-Belmonte et al., 1991). The Hox clock continues to operate after gastrulation and until the end of somitogenesis, within a posterior growth zone located in/around the caudal lateral epiblast-late primitive streak and later the tail bud (Deschamps & Duboule, 2017, Wymeersch et al., 2019, Wymeersch et al., 2021). The colinear activation of Hox genes within these posterior regions is thought to be tightly coupled to the assignment of the terminal A-P coordinates of the cell lineages that make up the postcranial axis, including the NC (Deschamps & Duboule, 2017, Wymeersch et al., 2019, Wymeersch et al., 2021). Eventually, the terminal expression domains of Hox genes along the A-P axis corresponds to their ordering within their chromosomal clusters so that the earliest activated, 3' Hox PG members are expressed more anteriorly compared to their later-activated 5' counterparts. In the case of NC, anterior cranial NC is Hox-negative, posterior cranial NC cells express Hox PG(1-3) genes, while vagal NC cells are marked by the expression of Hox PG(3-5) members and positivity for Hox PG(5-9) genes denotes a trunk NC character (Rocha et al., 2020).

The post-gastrulation posterior growth region is marked by high levels of Wnt/Fgf signalling activity and harbours a pool of multipotent axial progenitors driving embryonic axis elongation in a head-tail direction. These include neuromesodermal progenitors (NMPs) that generate a large fraction of the spinal cord as well as presomitic/paraxial mesoderm, the building blocks of the musculoskeleton (reviewed in (Henrique et al., 2015, Wymeersch et al., 2021). NMPs are marked by the co-expression of neural and mesodermal genes, such as those encoding the transcription factors *Sox2* and *Brachyury (T)* (Guillot et al., 2021, Henrique et al., 2015, Martin & Kimelman, 2012, Olivera-Martinez et al., 2012, Tsakiridis et al., 2014), as well as a number of other posteriorly expressed genes such as *Nkx1-2*, *Cdx2, Tbx6* and *Hox* family members (Amin et al., 2016, Dias et al., 2020, Gouti et al., 2017, Guillot et al., 2021, Javali et al., 2017, Koch et al., 2017, Rodrigo Albors et al., 2018, Wymeersch et al., 2019, Young et al., 2009).

Fate mapping, lineage tracing and single cell transcriptomics studies in vertebrate embryos have revealed that trunk NC cells, which give rise to neuroblastoma (the most common extracranial solid tumour in infants) following oncogenic transformation, are derived from NMPs (Javali et al., 2017, Lukoseviciute, 2021, Shaker et al., 2021, Tzouanacou et al., 2009, Wymeersch et al., 2016). Moreover, recent work has demonstrated that the *in vitro* generation of trunk NC cells and their derivatives from hPSCs relies on the induction of a NMP-like intermediate following stimulation of WNT/FGF signalling pathways (Abu-Bonsrah et al., 2018, Cooper, 2020, Faustino Martins et al., 2020, Frith et al., 2018, Frith & Tsakiridis, 2019, Gomez, 2019, Hackland et al., 2019, Kirino et al., 2018). These and other studies have pointed to a model where a generic posterior axial identity is installed early within the

NMP precursors of trunk NC cells under the influence of WNT/FGF activities prior to their differentiation and commitment to a NC fate (Frith et al., 2018, Metzis et al., 2018). However, it is unclear whether induction of a developmentally plastic, Brachyury-positive state is an obligatory step in the 'posteriorisation' of prospective NC cells or trunk NC cells can still acquire a posterior axial identity without passing through a mesoderm-competent progenitor stage.

Here we dissect the links between human NMP induction and trunk NC specification using hPSC differentiation as a model. We show that disruption of NMP ontogeny via knockdown of the NMP/mesoderm regulator TBXT (the human homologue of Brachyury) abolishes the acquisition of a posterior axial identity by NC cells without affecting adoption of an NC fate. This is linked to a failure of WNT-FGF-treated hPSCs to activate properly the expression of HOX genes. We demonstrate that TBXT mediates early posteriorisation by directly orchestrating an open chromatin landscape in HOX clusters and key WNT signalling-linked loci. In contrast, control of trunk HOX gene expression/posteriorisation in NMP-derived early central nervous system (CNS) spinal cord progenitors appears to be TBXT/WNT-independent and programmed after NMP differentiation primarily under the action of FGF signalling. Collectively, our data reveal a previously unappreciated role for TBXT in prospectively shaping the A-P patterning of NC cells. They also indicate the existence of two distinct phases of posterior axial identity control: (i) an early NMP-based that involves the TBXT/WNT-driven establishment/fixing of a HOX-positive, posterior character in uncommitted progenitors followed by its "transmission" to their downstream trunk NC derivatives and, (ii) a later one, which is based on the FGF-driven sculpting of a posterior axial identity in cells transiting toward a spinal cord neural fate, post-NMP differentiation.

Results

TBXT controls posterior axial identity acquisition by NMP-derived neural crest cells

We have previously described the *in vitro* generation of human neuromesodermal (NM)-potent cell populations resembling embryonic NMPs, following a 3-day treatment of hPSCs with the WNT agonist CHIR99021 (CHIR) and FGF2 (Frith et al., 2018, Gouti et al., 2014). We showed that $TBXT^+$ hPSC-derived NMPs give rise to TBXT-negative early trunk NC cells (marked by the expression of HOX PG(1-9) members/CDX2 together with NC markers such as SOX10) following re-plating and further 5-day culture in the presence of CHIR and controlled levels of BMP signalling (Frith et al., 2018, Frith & Tsakiridis, 2019). We hypothesised that if acquisition of a posterior axial identity by hPSC-derived trunk NC cells relies on the induction of NM-potent progenitors then early disruption of NMP induction/mesoderm formation competence should impair subsequent NC posteriorisation.

To test this, we examined the effects of attenuating TBXT, a well-established regulator of NMP maintenance and mesodermal differentiation (Amin et al., 2016, Gouti et al., 2014, Guibentif et al., 2021, Koch et al., 2017, Martin & Kimelman, 2010, Rashbass et al., 1991) using a human embryonic stem cell (hESC) line engineered to exhibit shRNA-mediated, tetracycline (Tet)-inducible knockdown of *TBXT* expression (Bertero et al., 2016). We confirmed that Tet addition during the differentiation of these hESCs toward NMPs induced a considerable reduction in TBXT expression both at the transcript and protein level compared to untreated controls (**Fig. 1A-D**). No effect on TBXT induction was observed in NMPs generated from an isogenic control Tet-inducible shRNA hESC line targeting the *B2M* gene (Bertero et al., 2016) following Tet treatment (**Fig. EV1A**).

To define the impact of TBXT depletion during the transition of hPSCs toward an NMP state, we carried out transcriptome analysis of Tet-treated and control hESCs cultured in NMP-inducing conditions (i.e. presence of CHIR and FGF2) for 3 days, using RNA sequencing (RNA-seq). We found that 346 and 293 genes were significantly up- and down-regulated respectively in TBXT knockdown cells compared to untreated controls (P adj<0.05, Wald test; log2FC > |0.5|)) (**Appendix Table S1**). Gene Ontology (GO) biological processes enrichment analysis revealed that most differentially expressed genes were established regulators of A-P regionalisation/posterior development (**Fig. 1E, Appendix Table S2**). Significantly downregulated genes included presomitic mesoderm-associated transcription factors (*TBX6*, *MSGN1*, *FOXC1/2*) as well as WNT (e.g. *RSPO3, WISP1, WNT5A/B, WNT8A, LEF1*), FGF (FGF3/8/17, *DUSP7*) and NOTCH (*HES7, DLL1/3*) signalling pathway-linked transcripts (**Fig. 1F, Appendix Table S1)**, most of which have been reported to be present in NMPs and their immediate mesodermal derivatives *in vivo* (Guillot et al., 2021, Koch et al., 2017, Wymeersch et al., 2019). Moreover, we found that TBXT knockdown triggered a reduction in the expression of various HOX genes belonging to anterior, central and posterior PG(1-9) (**Fig. 1G, Appendix Table S1**) while no effect was observed in Tet-treated *B2M* shRNA hESC-derived NMPs (**Fig. EV1B**) ruling out the possibility that the observed decrease in HOX transcript levels may be due to nonspecific effects of Tet and/or interference of shRNAs with the micro RNA processing machinery. On the contrary, the most-highly upregulated genes included anterior visceral endoderm (AVE)/endoderm, anterior neurectoderm and pluripotency/early post-implantation epiblast-associated genes such as *SOX17*, *LEFTY1/2*, *OTX2*, *CER1*, *HHEX*, *NANOG* and *GDF3* (**Fig. 1F, Appendix Table S1)**. Taken together, these results indicate that TBXT knockdown severely impairs the induction of NMPs and their immediate presomitic mesoderm progenitor derivatives from hPSCs. They also suggest that TBXT directs the establishment of a “posteriorising” signalling environment associated with early HOX gene activation, upon pluripotency exit,

since in its absence hPSCs adopt an identity that resembles the anterior epiblast despite the combined presence of caudalising WNT (CHIR) and FGF (FGF2) signalling agonists.

We next assessed the effect of TBXT disruption/failure to induce NMPs/presomitic mesoderm on trunk NC specification. To this end, we attempted to generate trunk NC cells from TBXT inducible shRNA hESCs via an NMP intermediate, treating cells initially with CHIR-FGF2 for 3 days to induce NMPs, followed by their re-plating under NC-promoting conditions (i.e. low CHIR and moderate BMP levels) for a further 5 days, as previously described (Frith et al., 2018, Frith & Tsakiridis, 2019), and either in the continuous presence or absence of Tet (**Fig. 2A**). We found that the expression of most HOX PG(1-9) genes examined was dramatically reduced in the resulting Tet-treated cultures compared to their untreated counterparts (**Fig. 2B, C**) indicating that failure of TBXT-depleted NMPs to induce properly HOX gene expression persists in their NC derivatives. The expression levels of *CDX2*, an early trunk NC regulator (Sanchez-Ferras et al., 2016, Sanchez-Ferras et al., 2012) were also found to be severely decreased (**Fig. 2D**). A modest but statistically significant reduction in the levels some NC-associated transcripts such as *SOX10* and *PAX3* was observed in the presence of Tet (P value<0.05 and <0.01 respectively; paired t-test) (**Fig. 2D**) though no obvious changes in SOX10 protein levels were detected (**Fig. 2E**). We also observed a trend towards a slight upregulation in the expression of the anterior neural crest markers *OTX2* and *ETS1* (Simoes-Costa & Bronner, 2016) as well as the neural progenitor marker *SOX1* (Wood & Episkopou, 1999) following TBXT knockdown (**Fig. 2D**). Based on these data we conclude that the acquisition of a posterior axial identity by trunk NC cells occurs at an early stage, prior to the emergence of SOX10^{+} definitive NC cells from NMPs. Intriguingly, this process is shaped by the action of TBXT, an NMP/pro-mesodermal regulator.

Early encoding of a posterior axial identity in NMP-derived neural crest cells is primarily WNT-dependent

Our RNA-seq data revealed the concomitant downregulation of WNT targets and upregulation of WNT antagonists (e.g. *DKK4*) in day 3 FGF-CHIR-treated cultures in the presence of Tet (**Appendix Table S1**, **Fig. 1F)** suggesting that the inability of TBXT-depleted NC cells to activate HOX genes may be linked to an early reduction in WNT activity. This is further supported by our observation that TBXT knockdown-triggered reduction of HOX gene expression in our NC cultures was also accompanied by a significant reduction in the expression of WNT signalling target genes such as *TCF1*, *LEF1* and *CDX2* (**Fig. 2D**). We therefore sought to determine the temporal effects of WNT signalling on posterior axial identity acquisition during the transition from hPSCs to NMPs and subsequently NC. We first assessed the effects of WNT signalling inhibition during the 3-day

induction of NMPs from hPSCs, by removing CHIR and treating the cultures with the tankyrase inhibitor XAV939 (XAV) (Huang et al., 2009) in order to eliminate any endogenous paracrine signalling, in the presence of FGF2 (the other major signalling agonist included in the media) (**Fig. 3A**). Given the reported role of FGF signalling in controlling the HOX clock in NMPs and their derivatives (Delfino-Machin et al., 2005, Hackland et al., 2019, Liu et al., 2001, Mouilleau et al., 2021, Nordstrom et al., 2006), we also tested the effect of attenuating this pathway in a similar manner, by omitting FGF2 and culturing cells only in the presence of CHIR and the FGF pathway-MEK1/2 inhibitor PD0325901 (PD03) between days 0-3 (**Fig. 3A**). Signalling inhibition was verified by confirming the downregulation/extinction of WNT (*AXIN2*, *TCF1*, *LEF1*) and FGF signalling target genes (*SPRY4*) in inhibitor-treated day 3 cultures relative to untreated controls (**Fig. 3B**). Our results confirmed that maximal induction of NMP markers (*TBXT*, *CDX2* and *NKX1-2*) and all HOX genes examined can be achieved only in the combined presence of WNT and FGF agonists (**Fig. 3C, 3D**, white bars). However, WNT signalling stimulation alone, in the absence of any FGF activity, rescued the induction of most HOX genes and *TBXT*/*CDX2* with variable efficiency (**Fig. 3D**, red bars) indicating that WNT is the main instructive pathway controlling the HOX clock and expression of major axis elongation regulators during the differentiation of hPSCs toward NMPs. HOXC genes were an exception, as their activation was found to be equally dependent on WNT and FGF signalling (**Fig. 3D**) suggesting the additional existence of HOX cluster-specific modes of transcriptional control, in line with similar findings in the embryo (Ahn et al., 2014, van den Akker et al., 2001).

We next examined the signalling pathway dependence of HOX gene expression during the transition of NMPs toward trunk NC cells, which involves a 5-day treatment with a lower amount of the WNT agonist CHIR and an intermediate level of BMP activity; the latter is achieved through the addition of a saturating amount of recombinant BMP4 together with the BMP type I receptor inhibitor DMH-1 to antagonistically modulate the effects of BMP4 (**Fig. 3E**) (Frith et al., 2018, Frith & Tsakiridis, 2019, Hackland et al., 2017). We examined the effect of perturbing the two main signalling pathways driving the specification of NC from NMPs (WNT and BMP) using agonist/antagonist combinations between days 3-8, in a manner similar to the day 0-3 treatments (**Fig. 3E**). Treatment of differentiating NMPs with XAV to inhibit WNT signalling in combination with BMP stimulation, resulted in a reduction in the expression of most HOX genes analysed albeit to a lesser degree compared to days 0-3 (**Fig. 3F,** dark blue vs purple bars). This was accompanied by a moderate increase in the expression of anterior (*OTX2*, *ETS1*) and decrease in posterior (*CDX2*) NC markers while the levels of neural/NC-specific transcripts appeared unaffected (**Fig. 3G,** dark blue vs purple bars). On the contrary, WNT stimulation in combination with the BMP inhibitor LDN193189 (LDN) had no effect or resulted in upregulation in the expression of most HOX

genes relative to the WNT-BMP controls (**Fig. 3F,** light blue vs purple bars). Moreover, this treatment resulted in complete extinction of the expression of the definitive neural crest marker *SOX10* and a concomitant increase in the expression of the neural progenitor marker *SOX1* (**Fig. 3G,** light blue vs purple bars) pointing to a role for BMP signalling in steering NMPs/dorsal pre-neural progenitors toward a NC fate in agreement with previous observations (Leung et al., 2016). Taken together, our results demonstrate that HOX gene activation in hPSC-derived NMPs and its tight coupling to the early programming of a posterior axial identity in NMP-derived NC cells are primarily driven by a WNT-TBXT loop. However, the early dependence of HOX gene expression on WNT signalling appears to diminish with time as NMPs gradually differentiate toward NC.

We went on to examine whether the reliance of early trunk NC progenitor patterning on WNT signalling occurs *in vivo*. Homotopic grafting-based fate mapping has indicated that NM-potent cells in the lateral-most caudal epiblast of somitogenesis-stage mouse embryos (marked as "LE" in **Fig. 4**) can give rise to posterior NC (Wymeersch et al., 2016). We examined *R26-WntVis* embryos, in which graded nuclear EGFP expression relates to the degree of WNT signalling strength (Takemoto et al., 2016), at the time of posterior NC formation (Embryonic day (E) 8.75-E9.0, Theiler stage 13-14). In agreement with previous work (Ferrer-Vaquer et al., 2010), the highest levels of Wnt activity were confined within the posterior growth region, whereas anteriorly only cells in the head mesenchyme exhibited medium levels of EGFP (**Fig. 4A**). As the axis grows, posterior trunk tissue (such as the somites) were also found to display high EGFP expression (**Fig. 4A**). Wholemount immunostaining and 3D modelling of the highest EGFP-positive fraction (a-GFP^{high}) demonstrated that NC-fated regions within the T(Brachyury)$^{+}$ lateral-most caudal epiblast domain are marked by higher WNT signalling levels compared to more medial positions (dashed lines in **Fig. 4B**, **EV2A-B**). Expression of Tfap2a, a marker indicative of early NC specification (Mitchell et al., 1991, Rothstein & Simoes-Costa, 2020) was first detected within the Wnt^{high} LE domain at E9.0 , whereas before it was only present in the non-neural ectoderm (compare arrows in **Fig. 4Ce-f** vs **4Cm-o**). At E8.75, Wnt activity levels appeared lower within committed, Sox9^{+} pre-migratory NC cells located in the dorsolateral neural tube (**Fig. 4Cc-d; EV2C**). However, E9.0 delaminating trunk NC and cranial NC cells were found to exhibit progressively elevated Wnt activity (**Fig. 4Cg-i** and **4CJ-l; EV2C**) reflecting the well-established role of this signalling pathway in promoting NC delamination and subsequent migration (Azambuja & Simoes-Costa, 2021, Burstyn-Cohen et al., 2004, Gandhi et al., 2020, Liu et al., 2013). Together these findings demonstrate that early specification of NM-potent TBXT^{+} trunk NC progenitors correlates with high WNT activity but this association becomes less prevalent as they gradually commit to a definitive, pre-migratory NC fate in line with our *in vitro* observations showing the early but progressively

297 decreasing WNT-dependence of TBXT-driven posterior axial identity programming in NC
298 cells.
299
300 **TBXT controls posterior axial identity acquisition by influencing chromatin**
301 **accessibility**
302 We next examined whether TBXT controls HOX gene activation and potentiates the action of
303 posteriorising extrinsic signals in CHIR-FGF-treated hPSCs via direct genomic binding or,
304 indirectly, by regulating the expression of other key posteriorising regulators such as CDX2.
305 To this end, we carried out chromatin immunoprecipitation followed by high-throughput
306 sequencing (ChIP-seq) on hPSC-derived NMPs and undifferentiated hPSCs (control) to map
307 TBXT targets genome-wide. We identified 24,704 TBXT-binding regions in NMPs (**Appendix**
308 **Table S3, Fig. EV3A**), a large fraction of which were located within introns (~50%) and distal
309 intergenic (~38%) regions (**Fig. EV3B**), reflecting similar findings on mouse T binding
310 (Beisaw et al., 2018, Tosic et al., 2019). A small number (n=2088) of non-overlapping TBXT
311 binding sites was also detected in undifferentiated hESCs, in line with the reported low-level
312 expression of this transcription factor in mesoderm-biased pluripotent cells (Stavish et al.,
313 2020, Tsakiridis et al., 2014). GO biological processes enrichment analysis of target genes
314 associated with TXBT binding sites around the transcriptional start site (-2000 to +500 bp;
315 3084 peaks, 2841 genes) revealed an over-representation of established developmental
316 regulators of A-P regionalisation (Benjamini–Hochberg P adj<0.05; **Fig. EV3C, Appendix**
317 **Table S4**). Transcription factor motif enrichment analysis revealed that the TBXT binding
318 regions in hPSC-derived NMPs were enriched, as expected, for the Brachyury consensus
319 binding motif as well as other T-BOX binding motifs such as EOMES and TBX6 (**Fig. 5A,**
320 **Appendix Table S5**), in agreement with previous findings in the mouse demonstrating that a
321 fraction of the genomic targets of these transcription factors is also occupied by TBXT (Koch
322 et al., 2017, Tosic et al., 2019). Other over-represented motifs included WNT signalling
323 effectors (LEF1/TCF3) and Homeobox genes such as CDX factors (CDX2/4) and various
324 HOX family members (**Fig. 5A, Appendix Table S5**) reflecting possible cooperative binding
325 between these factors and TBXT in human NMPs. Comparison of TBXT ChiP-seq targets
326 with our list of differentially expressed genes following Tet-induced TBXT knockdown in day
327 3 FGF-CHIR treated cultures (**Fig. 1**) revealed that the majority (~85%) of the downregulated
328 (P adj <0.05, log2FC > |1|) genes, including HOX PG(1-9) members, pro-mesodermal
329 factors and WNT-FGF signalling components, were directly bound by TBXT, while most
330 (~60%) of their upregulated counterparts were not (**Fig. 5B, 5C, 5F, EV3D, Appendix Table**
331 **S6)**. This indicates that TBXT acts primarily as a transcriptional activator of key downstream
332 NMP/mesoderm regulators and HOX genes as previously reported (Amin et al., 2016,
333 Beisaw et al., 2018, Guibentif et al., 2021, Koch et al., 2017, Lolas et al., 2014).

To further dissect the impact of TBXT binding, we interrogated the chromatin accessibility landscape in TBXT-depleted and control hPSC-derived NMPs using ATAC-seq (assay for transposase accessible chromatin with high-throughput sequencing) (Buenrostro et al., 2013). We detected 4421 and 4027 unique regions corresponding to loss or gain of chromatin accessibility following Tet treatment, respectively (distance from TSS ranging from -1 to 1 kb, log2FC cutoff = 2 and p-value < 0.05) (**Fig. 5D, Appendix Table S7**). Genes associated with loss of chromatin accessibility were predominantly linked to A-P patterning, mesoderm specification and WNT signalling (**Appendix Table S7**). Moreover, the Tet-induced downregulation of most transcripts found to be TBXT targets (**Appendix Table S3**) was also accompanied by a significant loss of 'open' chromatin regions within the TBXT binding sites (**Fig. 5E, 5F, Appendix Table S7**). These included sites that were dispersed within all HOX clusters as well as key presomitic mesoderm regulators (e.g. TBX6, MSGN1) and WNT signalling components (e.g. WNT3A/8A, LEF1) (**Fig. 5F, EV3D**). On the contrary, there was no obvious correlation between upregulation of expression following TBXT knockdown and chromatin accessibility change (**Fig. 5E, Appendix Table S7**). Gain of accessible regions in TBXT-depleted hPSC-derived NMPs appeared to occur predominantly within/around loci linked to neural development (e.g. SOX3 and DLG2 (Tao et al., 2003, Wood & Episkopou, 1999)), most of which were not bound directly by TBXT (**Fig. 5G, Appendix Table S7**). Moreover, examination of transcription factor binding motifs (annotated using HOMER (Heinz et al., 2010); Benjamini–Hochberg P adj<0.05) showed that ATAC-seq sites marked by loss of chromatin accessibility following TBXT knockdown were uniquely enriched in CDX, T-box factor and HOX binding-associated DNA sequence elements whereas the regions marked by gain of chromatin accessibility were mainly characterised by motifs indicating binding of SOX, OCT/POU and Forkhead family transcription factors (**Fig. EV3E, Appendix Table S8**). Collectively, these data suggest that TBXT actively reconfigures the chromatin landscape in HOX genes and other axis elongation regulators, including WNT signalling components, by direct binding to key regulatory elements to promote the acquisition of a posterior axial character/mesoderm identity during the transition of pluripotent cells toward a caudal epiblast/NMP state.

Posterior axial identity acquisition by NMP-derived pre-neural spinal cord cells is TBXT-independent and FGF-dependent

We next sought to examine whether early TBXT knockdown-triggered disruption of HOX gene expression/NMP induction also affects the CNS derivatives of NMPs. We thus generated early pre-neural spinal cord progenitors, which we have recently shown to give rise to posterior motor neurons of a thoracic axial identity, from TBXT shRNA hESCs (Wind et al., 2021). Cells were treated with CHIR-FGF2 for 3 days followed by their re-plating and

371 further culture in the presence of CHIR and high FGF levels for 4 days combined with
372 continuous Tet treatment to mediate TBXT knockdown (**Fig. 6A**). The levels of most HOX
373 transcripts examined were largely unaffected in day 7 pre-neural spinal cord progenitors
374 generated from TBXT-depleted cells, and similar to untreated controls (**Fig. 6B**). No
375 dramatic changes in the expression of *CDX2* and *SOX2* (markers of an early spinal cord
376 character at this stage) were observed (**Fig. 6C**). In line with our previous observations and
377 published *in vivo* data (Gofflot et al., 1997, Nordstrom et al., 2006, Wind et al., 2021), we
378 also detected low levels of TBXT transcripts in control cultures and, surprisingly, these were
379 comparable to their Tet-treated counterparts (**Fig. 6C**). This finding suggests that selection
380 of cells evading shRNA knockdown and maintaining low levels of *TBXT* may occur upon
381 culture in pre-neural spinal cord cell-promoting culture conditions. Later addition of Tet at
382 day 3, at the start of NMP differentiation toward pre-neural spinal cord cells, appeared to
383 restore efficient TBXT knockdown (**Fig. 6D, F**) but, again, had no major impact on either
384 HOX PG(1-9) gene expression or the levels of the early spinal cord/pre-neural transcripts
385 *CDX2* and *NKX1-2* in the resulting day 7 cultures (**Fig. 6E, F**). These results indicate that, in
386 contrast to NMP-derived NC, HOX expression dynamics/posterior axial identity in NMP-
387 derived pre-neural spinal cord cells are unlikely to be controlled by TBXT.
388 Both WNT and FGF signalling have been previously implicated in the control of the
389 Hox clock/early posterior patterning of spinal cord cells, through cooperation with the key
390 axis elongation factor Cdx2 (Bel-Vialar et al., 2002, Lippmann et al., 2015, Liu et al., 2001,
391 Mazzoni et al., 2013, Metzis et al., 2018, Mouilleau et al., 2021, Nordstrom et al., 2006,
392 Olivera-Martinez et al., 2014, Takemoto et al., 2006, van de Ven et al., 2011). Our data so
393 far have demonstrated an early requirement for WNT signalling in inducing a posterior axial
394 identity/Hox activation during the transition of hPSCs toward NMPs. This reliance on WNT
395 signalling diminishes during the transition of NMPs toward an NC fate. We tested whether
396 this is also the case during the differentiation of NMPs toward pre-neural spinal cord
397 progenitors (following their re-plating in the presence of CHIR-high FGF2 levels). We carried
398 out signalling agonist/inhibitor combination experiments as described earlier (**Fig. 3**) treating
399 differentiating cells either with the WNT inhibitor XAV in the presence of FGF2 or the
400 FGF/MEK inhibitor PD03 in combination with CHIR between days 3-7 of differentiation (**Fig.**
401 **7A**). We found that WNT signalling inhibition in the presence of FGF activity during this time
402 window does not appear to have a major effect on HOX gene expression or *CDX2* levels
403 (blue bars in **Fig. 7B-D**). In contrast, blocking FGF signalling in combination with CHIR
404 treatment resulted in a dramatic reduction in the expression of most HOX genes examined,
405 particularly those belonging to PG(4-9), as well as *CDX2* (red bars, **Fig. 7B-D**). The
406 NMP/pre-neural spinal cord marker *NKX1-2* was equally affected by the two treatments
407 while the levels of later spinal cord markers (*PAX6*, *SOX1*) were modestly elevated (**Fig.**

7C). Collectively, these data suggest that HOX gene as well as CDX2 expression levels during the specification of early spinal cord cells from hPSC-derived NMPs rely primarily on FGF signalling and do not appear to depend on the action of an early NMP-based WNT-TBXT regulatory loop.

Discussion

A number of recent studies have demonstrated that the emergence of the trunk NC is tightly coupled to the induction of NM-potent progenitors localised in the post-gastrulation/somitogenesis stage posterior growth region of vertebrate embryos. Here we provide evidence indicating that the encoding of a posterior axial identity in human NC cells, embodied by the sequential activation of Hox genes and the induction of posterior markers, relies on their transition through this developmentally-plastic entity. This “primary regionalisation” process (Metzis et al., 2018) is mediated by the action of the pro-mesodermal transcription factor TBXT, which directs the operation of the Hox clock and the expression of posterior/presomitic mesoderm regulators together with WNT signalling effectors and, possibly, CDX2 (**Fig. 7E**). The early WNT dependence of trunk NC-associated Hox gene expression diminishes after NMP specification as definitive pre-migratory NC cells begin to emerge, before this signalling pathway becomes critical again in controlling later NC delamination/migration events. Strikingly, the expression of HOX genes, particularly those belonging to the central/posterior PG(4-9), in prospective posterior CNS spinal cord cells is mainly controlled by FGF signalling and appears unaffected by early HOX expression disruption events induced by TBXT depletion. This suggests that a separate NMP/TBXT/WNT-independent mechanism of Hox gene transcriptional control operates at a later post-NMP specification but pre-neural commitment stage, within this lineage (**Fig. 7E**).

Our proposed model synthesises previous findings showing that WNT-driven posterior axial identity acquisition in neural derivatives of NMPs takes place prior to neural induction (Lippmann et al., 2015, Metzis et al., 2018, Neijts et al., 2017, Neijts et al., 2016, Takemoto et al., 2006) with data illustrating that temporally discrete modes of trunk axial patterning in CNS spinal cord/NC rely on both FGF and WNT activities (Bel-Vialar et al., 2002, Delfino-Machin et al., 2005, Dunty et al., 2014, Gomez, 2019, Hackland et al., 2019, Liu et al., 2001, Mazzoni et al., 2013, Mouilleau et al., 2021, Muhr et al., 1999, Nordstrom et al., 2006, Sanchez-Ferras et al., 2016, Sanchez-Ferras et al., 2014, Sanchez-Ferras et al., 2012, van Rooijen et al., 2012, Zhao et al., 2014). Our work also reflects results showing the existence of distinct phases of Hox gene expression program implementation *in vivo*: (1) an early “plastic” phase linked to A-P patterning of multipotent axial progenitors/NMPs within their posterior niche and (2) a later phase, which marks the instalment and fixing of lineage-

specific Hox gene expression patterns and the sharpening of their final boundaries in the neural and mesodermal derivatives of axial progenitors as and after they exit the posterior growth zone (Ahn et al., 2014, Brend et al., 2003, Charite et al., 1998, Deschamps & Wijgerde, 1993, Forlani et al., 2003, Hayward et al., 2015, McGrew et al., 2008, Wymeersch et al., 2019).

We demonstrate that TBXT function is crucial for proper collinear activation of Hox genes during NMP induction from hPSCs *in vitro* by channelling extrinsic WNT activity toward the establishment of a "posteriorising"/pro-mesodermal niche (in line with previous data (Martin & Kimelman, 2010)) that is essential for the subsequent transduction of a posterior character to NMP-derived NC cells. This prospective TBXT-WNT-driven transmission of positional information via an early axial progenitor intermediate and the potential inductive interaction between nascent presomitic mesoderm and NC progenitors reinforces previous observations on the effect of non-organiser mesoderm and vertical signalling as determinants of HOX gene expression and axial identity in early neural cells (Bardine et al., 2014, Forlani et al., 2003, Grapin-Botton et al., 1997). However, further work is required to disentangle the cell vs non-cell autonomous effects of TBXT on the A-P patterning of NC cells.

Our results are in line with previous studies reporting that TBXT attenuation in hPSC-derived mesoderm progenitors and spinal cord organoids as well as in Xenopus morphant and mouse *Tc* (Curtailed) mutant embryos abolishes Hox gene expression (Faial et al., 2015, Libby et al., 2021, Lolas et al., 2014, Wacker et al., 2004). Moreover, they further expand the repertoire of actions that orchestrate embryonic axis elongation/axial progenitor ontogeny and are exerted via the regulatory axis centred on WNT signalling, TBXT and the Hox clock (Denans et al., 2015, Mariani et al., 2021, Ye et al., 2021, Ye & Kimelman, 2020). Interestingly, global Hox gene expression appears minimally affected in some Brachyury mutants (such as those with the $T^{2J/2J}$ genotype (Koch et al., 2017, Tosic et al., 2019)), as well as in $T^{-/-}$ :: Wild type chimeras (Guibentif et al., 2021) suggesting that the nature of the *T* gene mutation and non-cell autonomous rescue effects from the surrounding wild-type environment, similar to those described previously in the case of grafted *Cdx* mutant axial progenitors (Bialecka et al., 2010), are critical actors in influencing the effect of Brachyury on its target genes. Moreover, the developmental arrest exhibited by *T* mutant embryos around the time of trunk NC emergence and the associated lack of posterior axial tissue precludes detailed assessment of Hox gene expression in *T* null NC cells.

TBXT has been shown to regulate its downstream mesoderm/axis elongation-associated targets in mouse embryos by promoting chromatin remodelling and directing permissive chromatin modifications in key regulatory elements (Amin et al., 2016, Beisaw et al., 2018, Koch et al., 2017, Tosic et al., 2019). Our data confirm that this is also the case

during the transition of hPSCs toward NMPs and reveal that TBXT additionally contributes to global control of Hox cluster transcription in a similar way and in line with previous reports showing direct TBXT binding in Hox loci during hPSC differentiation (Faial et al., 2015). We propose that concomitant activation of the Hox clock and induction of WNT signalling components, via TBXT-driven chromatin landscape reconfiguration, comprise a critical early step in primary A-P regionalisation and the transition of pluripotent cells toward a caudal epiblast/axial progenitor state. This is supported by our demonstration that TBXT knockdown results in the acquisition of an anterior epiblast/AVE identity associated with WNT antagonism/head formation-promoting activity as well as increased chromatin accessibility in regulatory elements controlling pro-neural differentiation genes. Previous data on the crucial role of Brachyury in counteracting the default neurectodermal differentiation of mouse pluripotent cells by altering chromatin accessibility in key enhancers also point to such a model (Tosic et al., 2019). Moreover, early A-P regionalisation driven by the TBXT-WNT-HOX axis is likely to involve the cooperative action of CDX factors and the participation of other key transcriptional factors such as EOMES and SOX2 given their previously reported functions in the mouse (Amin et al., 2016, Blassberg, 2020, Metzis et al., 2018, Neijts et al., 2017, Neijts et al., 2016, Tosic et al., 2019). Thus, additional thorough dissection of the individual roles of these factors via loss-/gain of-function approaches is required in order to elucidate their crosstalk as they fine-tune the balance between pluripotency exit, cell fate decision making and adoption of a posterior character in human cells.

In summary, we provide a mechanistic insight into the cellular and molecular basis of posterior axial identity acquisition during hPSC differentiation. Our data demonstrate a novel role for TBXT in controlling Hox gene expression and early posteriorisation supporting the idea that A-P patterning of at least some axial progenitor derivatives, such as the trunk neural crest, occurs prior to their specification, within their multipotent precursors. We speculate that the close links between TBXT-driven posterior axial identity programming in the neural crest and NMP ontogeny may explain some cases of spina bifida observed in individuals carrying mutations within the TBXT locus (Agopian et al., 2013, Carter et al., 2011, Fellous et al., 1982, Morrison et al., 1996, Shields et al., 2000), especially in light of the potential involvement of impaired NC specification and HOX gene dysregulation in neural tube defects (Anderson et al., 2016, Degenhardt et al., 2010, Poncet et al., 2020, Rochtus et al., 2015, Yu et al., 2019).

Materials and Methods

Cell culture and differentiation

Use of hPSCs has been approved by the Human Embryonic Stem Cell UK Steering Committee (SCSC15-23). The *TBXT* and *B2M* shRNA sOPTiKD hESC lines (H9

519 background) (Bertero et al., 2016) were employed for all TBXT loss-of-function and
520 sequencing experiments whereas signalling agonist/antagonist treatments were performed
521 in H9 hESCs and SFCi55-ZsGr human induced PSCs (Lopez-Yrigoyen et al., 2018,
522 Thomson et al., 1998). All cell lines were cultured routinely in feeder-free conditions in either
523 Essential 8 (Thermo Fisher or made in-house) or mTeSR1 (Stem Cell Technologies)
524 medium on laminin 521 (Biolamina) or Geltrex LDEV-Free reduced growth factor basement
525 membrane matrix (Thermo Fisher). Cells were passaged twice a week after reaching
526 approximately 80% confluency using PBS/EDTA as a passaging reagent. TBTX inducible
527 knockdown in the *TBXT* shRNA sOPTiKD hESC line was achieved using tetracycline
528 hydrochloride (Merck Life Science) at 1µg/ml as described previously (Bertero et al., 2016).
529 hESCs were cultured in the presence/absence of tetracycline for 2 days prior to the initiation
530 of differentiation and the tetracycline treatment was continued throughout the differentiation
531 for the periods indicated in the results section/schemes.
532 For NMP differentiation, hPSCs (70-80% confluent) were dissociated using Accutase
533 solution (Merck Life Science) and plated at a density of approximately 50,000 cells/cm^2 on
534 vitronectin (Thermo Fisher)-coated culture plates in N2B27 basal medium containing 50:50
535 DMEM F12 (Merck Life Science / Neurobasal medium (Gibco) and 1x N2 supplement
536 (Gibco), 1x B27 (Gibco), 1x GlutaMAX (Gibco), 1x MEM NEAA (Gibco), 2-Mercaptoethanol
537 (50 µM, Gibco). N2B27 medium was supplemented with CHIR99021 (3 µM, Tocris), FGF2
538 (20 ng/ml, R&D Systems) and Rho-Associated Coil Kinase (ROCK) inhibitor Y-27632 2HCl
539 (10 µM, Adooq Biosciences) with the latter being withdrawn from the differentiation medium
540 after the first day of NMP induction. For TBXT inducible knockdown, NMP medium was
541 supplemented with 1µg/ml tetracycline hydrochloride and replenished every other day.
542 For early spinal cord progenitor differentiation, day 3 hPSC-derived NMPs were dissociated
543 into single cell suspension using Accutase and re-plated at a density of 37,500 cells/cm^2 on
544 Geltrex-coated culture plates in N2B27 containing FGF2 (100 ng/ml), CHIR99021 (3 µM)
545 and ROCK inhibitor Y-27632 2HCl (10 µM; for the first day only) in the presence or absence
546 of tetracycline hydrochloride (1µg/ml). Medium was replaced every other day until day 7 of
547 differentiation. For trunk neural crest differentiation, day 3 hPSC-derived NMPs were
548 dissociated using Accutase and re-plated at a density of 50,000 cells/cm^2 on Geltrex-coated
549 culture plates directly into neural crest inducing medium consisting of DMEM/F12, 1x N2
550 supplement, 1x GlutaMAX, 1x MEM NEAA, the TGF-beta/Activin/Nodal inhibitor SB-431542
551 (2 µM, Tocris), CHIR99021 (1 µM), BMP4 (15ng/ml, Thermo Fisher), the BMP type-I
552 receptor inhibitor DMH-1 (1 µM, Tocris) and ROCK inhibitor Y-27632 2HCl (10 µM). The
553 medium was refreshed every two days without ROCK inhibitor and was supplemented with
554 1µg/ml tetracycline hydrochloride throughout the differentiation for tet-mediated inducible
555 TBXT knockdown. Trunk neural crest cells were analysed at day 8 of differentiation. The

following signalling pathway inhibitors were employed: the WNT antagonist tankyrase inhibitor XAV 939 (1 μM, Tocris), the MEK1/2 inhibitor PD0325901 (1 μM, Merck), LDN-193189 (100 nM, Tocris).

Immunofluorescence and imaging

Cells were fixed in 4% PFA for 10 minutes at room temperature, rinsed twice with PBS and permeabilised with 0.5% Triton X-100 in PBS containing 10% Foetal Calf Serum (FCS) and 0.1% Bovine Serum Albumin (BSA) for 15 minutes. Blocking was then performed in blocking buffer consisting of 10% FCS, 0.1% BSA in PBS at room temperature for 1-2 hours or overnight at 4^0C. Primary antibodies were diluted in blocking buffer and cells were incubated with primary antibodies overnight at 4oC. Following three washes, cells were incubated with secondary antibodies diluted in blocking buffer for 1-2 hours at room temperature and in the dark. Cell nuclei were counterstained with Hoechst (Thermo Fisher, 1:1000) and fluorescent images were acquired using the InCell Analyser 2200 system (GE Healthcare). Images then were processed in Fiji (Schindelin et al., 2012) or Photoshop (Adobe) using identical brightness/contrast settings to allow comparison between different treatments. At all times, the positive/negative threshold was set based using a sample incubated with secondary antibody only. The following primary antibodies were employed: anti-TBXT (Abcam, ab209665; 1:1000); anti-CDX2 (Abcam, ab76541; 1:200); anti-HOXC9 (Abcam, ab50839; 1:50); anti-SOX10 (Cell Signalling Technology, D5V9L; 1: 500).

For quantification of TBXT protein expression in NMP-like cells, nine random fields per experiment were scored (two biological replicates) and processed in the image analysis software CellProfiler (Carpenter et al., 2006). Nuclei were first identified using Hoechst staining and subsequently mapped onto the other fluorescent channels for single-cell fluorescence intensity quantification. Cells stained with secondary antibody only were used as negative control to set the negative/positive threshold. A histogram was created using GraphPad Prism (GraphPad Software). For quantification of SOX10 and HOXC9 protein expression in trunk neural crest, 5 random fields per experiment were scored (3 biological replicates) and processed as described above.

Immunofluorescence analysis of wholemount embryos and 3D reconstruction

E8.75 and E9.0 (TS13-14) *R26-WntVis* embryos were dissected in-house prepared M2 medium (Nowotschin et al., 2010). Embryos with yolk sac and amnion removed were fixed for 25-30 minutes at 4°C in 4% PFA in PBS, followed by permeabilisation in 0.5% Triton X-100 in PBS for 15 minutes, then incubated in 0.5 M glycine in PBS in 0.1% Triton X-100 (PBST) for 20 minutes, after which they were washed three times in PBST and blocked overnight at 4°C in 10% serum (Merck) in PBS/0.3% TritonX100. Both primary and Alexa

Fluor®-conjugated secondary antibodies (Thermo Fisher Scientific and Alexa Fluor® 647 donkey-anti-chicken [#703-606-155] from Jackson Immunoresearch; all at 2 µg/ml final concentration) were diluted in blocking buffer and samples were incubated for 48 hours on a rocking platform at 4°C. A minimum of four 25-minute washes were performed with PBST on a rocking platform at room temperature after the primary and secondary antibody incubation. Antibodies used (supplier, final concentration): anti-GFP (Abcam; ab13970; 10 µg/ml); anti-Brachyury (R&D; AF2085; 1 µg/ml); anti-LB1 (Abcam; ab16048; 1:800-1:1000); anti-Sox9 (Merck, AB5535; 2 µg/ml); anti-Tfap2a (DSHB, 3B5, 3.1µg/ml). Embryos were counterstained with Hoechst33342 (Thermo Fischer Scientific; 5 µg/ml). Confocal microscopy was performed after dehydration through an increasing methanol/PBS series (25%, 50%, 75%, 10 min each) and two 5 min washes in 100% methanol and clearing in 1:1 v/v methanol/BA:BB (2:1 benzyl alcohol:benzyl benzoate; Sigma), and two washes in 100% BA:BB. Embryos were imaged in BA:BB under a LSM800 confocal system with Airyscan and GaAsP detectors (Zeiss). Two to three replicate embryos were imaged per staining and stage. Wholemount immunostaining data was processed using Zeiss or Imaris software (Oxford Instruments) using channel alignment, background subtraction and deconvolution tools. In Imaris, 3D volumes were created from single channels. These volumes represent positive stained areas, and - as volumes were allowed to merge - they do not represent cells. As many cells in the tail bud have some level of EGFP expression, only the fraction of a-GFP-stained cells with higher intensity (a-GFP^{high}) were displayed in the analyses for clarity reasons (compare a-GFP signal to 3D volumes in **EV2B-D**). The filtering of a-GFP^{low} 3D volumes was kept constant between different regions of individual embryos.

Quantitative real time PCR

Total RNA was extracted using the total RNA purification kit (Norgen Biotek) following manufacturer's instructions. CDNA preparation was completed using the High-Capacity cDNA Reverse Transcription kit (Thermo Fisher). Quantitative real-time PCR was carried out using the QuantStudio 12 K Flex (Applied Biosystems) thermocycler in combination with the Roche UPL system and the TaqMan Fast Universal PCR Master Mix (Applied Biosystems). Primer sequences are shown in Appendix Table S9.

Mouse husbandry

All mice were maintained on a 12 hr-light/12 hr-dark cycle and housed in 18–23 °C with 40–60% humidity. Homozygote *R26-WntVis* mice were obtained from the Laboratory for Animal Resources and Genetic Engineering at the RIKEN Center for Biosystems Dynamics Research, Kobe, Japan (accession no. CDB0303K; RBRC10162). Homozygote *R26-WntVis* males were crossed with ICR females (JAX stock #009122, The Jackson Laboratory); all

experiments were performed on heterozygote embryos. For timed matings, noon on the day of finding a vaginal plug was designated E0.5. All animal experiments were approved by the Institutional Animal Experiments Committee of RIKEN Kobe Branch. Mice were handled in accordance with the ethics guidelines of the institute

RNA-seq

Sample preparation

Total RNA was harvested from day 3 NMPs obtained from *TBXT* shRNA sOPTiKD hESC in the presence and absence of Tetracycline (three biological replicates) using the total RNA purification plus kit (Norgen BioTek) according to the manufacturer's instructions. Sample quality control, library preparation and sequencing were carried out by Novogene (http://en.novogene.com). Library construction was carried out using the NEB Next Ultra RNA Library Prep Kit and sequencing was performed using the Illumina NoveSeq platform (PE150). Raw reads were processed through FastQC v0.11.2 (https://www.bioinformatics.babraham.ac.uk/projects/fastqc/) and Trim Galore (https://www.bioinformatics.babraham.ac.uk/projects/trim_galore/). Reads were aligned using STAR v2.4.2a (Dobin et al., 2013) to the human reference genome assembly GRCh38 (Ensembl Build 79) in the two-pass mode. RSEM v1.3.0 (Li & Dewey, 2011) was used to extract expected gene counts, where genes expressed in < 3 samples or with total counts ≤ 5 among all samples were excluded. We identified genes showing significant differential expression with DESeq2 (Love et al., 2014), with log2FoldChange> |0.5| and Benjamini–Hochberg-adjusted P<0.05. Data were deposited to GEO (Accession number: GSE184622).

Chip-seq

Chromatin immunoprecipitation followed by next-generation sequencing (ChIP-seq) was performed on approximately 10 million cells/sample (three pooled replicates per sample), fixed with 1% formaldehyde solution (11% formaldehyde, 0.1M NaCl, 1mM EDTA (pH 8.0), 50mM HEPES (pH 7.9)) for 15 minutes at room temperature on a shaking apparatus. Fixation was quenched with 125mM of glycine (1/20 volume of 2.5M stock) for 5 minutes and then adherent cells were scraped thoroughly from the culture surface. Cells were washed, centrifuged at 800 x g for 10 minutes at 4^{o}C and pellets were resuspended in 10ml chilled PBS-Igepal (1X PBS (pH 7.4), 0.5% Igepal CA-630). This pellet wash was repeated and cells were resuspended in 10 ml chilled PBS-Igepal and 1mM PMSF. Samples were centrifuged at 800 x g for 10 minutes at 4^{o}C for a third time, after which the supernatant was removed and pellets were snap-frozen on dry ice and stored at -80^{o}C. Samples were sent to Active Motif (Carlsbad, CA) for ChIP-seq. Active Motif (https://www.activemotif.com) prepared the chromatin, performed ChIP reactions, generated libraries, sequenced them and

667 performed basic data analysis. Chromatin was isolated by adding lysis buffer, followed by
668 disruption with a Dounce homogenizer. Lysates were sonicated and the DNA sheared to an
669 average length of 300-500 bp with Active Motif's EpiShear probe sonicator (cat# 53051).
670 Genomic DNA (Input) was prepared by treating aliquots of chromatin with RNase, proteinase
671 K and heat for de-crosslinking, followed by SPRI beads clean up (Beckman Coulter) and
672 quantitation by Clariostar (BMG Labtech). Extrapolation to the original chromatin volume
673 allowed determination of the total chromatin yield. An aliquot of chromatin (50 µg) was
674 precleared with protein G agarose beads (Invitrogen) and genomic DNA regions of interest
675 were isolated using 4 µg of antibody against Brachyury (R&D Systems, cat# AF2085, lot#
676 KQP0719121). Complexes were washed, eluted from the beads with SDS buffer, and
677 subjected to RNase and proteinase K treatment. Crosslinks were reversed by incubation
678 overnight at 65^{o}C, and ChIP DNA was purified by phenol-chloroform extraction and ethanol
679 precipitation. Quantitative PCR (QPCR) reactions were carried out in triplicate on specific
680 genomic regions using SYBR Green Supermix (Bio-Rad). The resulting signals were
681 normalized for primer efficiency by carrying out QPCR for each primer pair using Input DNA.
682 Illumina sequencing libraries were prepared from the ChIP and Input DNAs by the standard
683 consecutive enzymatic steps of end-polishing, dA-addition, and adaptor ligation. Steps were
684 performed on an automated system (Apollo 342, Wafergen Biosystems/Takara). After a final
685 PCR amplification step, the resulting DNA libraries were quantified and sequenced on
686 Illumina's NextSeq 500 (75 nt reads, single end). Reads were aligned to the human genome
687 (hg38) using the BWA algorithm (default settings) (Li & Durbin, 2009). Duplicate reads were
688 removed and only uniquely mapped reads (mapping quality >25) were used for further
689 analysis. Alignments were extended in silico at their 3'-ends to a length of 200 bp, which is
690 the average genomic fragment length in the size-selected library, and assigned to 32-nt bins
691 along the genome. The resulting histograms (genomic "signal maps") were stored in bigWig
692 files. Peak locations were determined using the MACS algorithm (v2.1.0) (Zhang et al.,
693 2008) with a cutoff of p-value = 1e-7. Peaks that were on the ENCODE blacklist of known
694 false ChIP-Seq peaks were removed. Signal maps and peak locations were used as input
695 data to Active Motifs proprietary analysis program, which creates Excel tables containing
696 detailed information on sample comparison, peak metrics, peak locations and gene
697 annotations. Motif analysis was carried out using the Homer software (Heinz et al., 2010).
698 Regions of 200 bp surrounding the summit of the top 2,500 peaks (based on MACS2 p-
699 values) were analysed. Data were deposited to GEO (Accession number: GSE184622).
700
701 **ATAC-seq**
702 Day 3 NMPs (50,000 cells) obtained from *TBXT* shRNA sOPTiKD hESC in the presence and
703 absence of Tetracycline (three biological replicates) were harvested and samples were

prepared using the Illumina Tagment DNA Enzyme and Buffer Small Kit (Illumina), 1% Digitonin (Promega) and EDTA-free Protease Inhibitor cocktail (Roche). Following DNA purification with the MinElute kit eluting in 12 µl, 1 µl of eluted DNA was used in a quantitative PCR (qPCR) reaction to estimate the optimal number of amplification cycles. The remaining 11 µl of each library were amplified for the number of cycles corresponding to the Cq value (i.e., the cycle number at which fluorescence has increased above background levels) from the qPCR. Library amplification was followed by AMPure beads (Beckman Coulter) size selection to exclude fragments smaller than 150bp and larger than 1,200 bp. Library amplification was performed using custom Nextera primers. DNA concentration was measured with a Qubit fluorometer (Life Technologies) and library profile was checked with Bioanalyzer High Sensitivity assay (Agilent Technologies). Libraries were sequenced by the Biomedical Sequencing Facility at CeMM (Research Center for Molecular Medicine of the Austrian Academy of Sciences, Vienna) using the Illumina HiSeq 3000/4000 platform and the 50-bp single-end configuration. Base calling was performed by Illumina Real Time Analysis (v2.7.7) software and the base calls were converted to short reads using the IlluminaBasecallsToSam tool from the Picard toolkit (v2.19.2) ("Picard Toolkit." 2019. Broad Institute, GitHub Repository. http://broadinstitute.github.io/picard/; Broad Institute). Sequencing adapters were removed, and the low-quality reads were filtered using the fastp software (v 0.20.1) (Chen et al., 2018). Alignment of the short reads on GRCh38 was performed using Bowtie2 (v2.4.1) (Langmead & Salzberg, 2012) with the "-very-sensitive" parameter. PCR duplicates were marked using samblaster (v0.1.24) (Faust & Hall, 2014), and the reads mapped to the ENCODE black-listed (Amemiya et al., 2019) regions were discarded prior to peak calling. To detect the open chromatin regions, we performed peak calling using the MACS2 (v2.2.7.1) (Zhang et al., 2008) software with the "--nomodel", "--keep-dup auto" and "--extsize 147" options. Peaks in the format of bed files were analysed for differential analysis to compare signals corresponding to the + vs –Tet samples using the GUAVA software. Differential peaks with a distance from TSS ranging from -1 to 1 kb, log2FC cutoff = 2 and p-value < 0.05 were extracted. Finally, HOMER findMotifs (v4.11) (Heinz et al., 2010)was used for motif enrichment analysis over the detected open chromatin regions. Data were deposited to GEO (Accession number: GSE184227).

Acknowledgements

We wish to thank Prof. Ludovic Vallier (University of Cambridge) for providing the *TBXT* and *B2M* shRNA sOPTiKD hESC lines and Prof. Lesley Forrester (University of Edinburgh for providing the SFCi55-ZsGr iPSC line. We would also like to thank the Biomedical Sequencing Facility at CeMM/Michael Schuster and Leonardo Mottta, Estelle Suaud/Active Motif for assistance with the ATAC-seq and ChiP-seq experiments respectively. Finally, we

are grateful to James Briscoe, Fay Cooper, Vicki Metzis, Matt Towers and Val Wilson for critical reading of the manuscript.

Funding

This work has been supported by funding to AT from the Biotechnology and Biological Sciences Research Council (New Investigator Research Grant, BB/P000444/1), the European Union Horizon 2020 Framework Programme (H2020-EU.1.2.2; grant agreement ID 824070), Children's Cancer and Leukaemia Group/Neuroblastoma UK (CCLGA 2019 28) and the Medical Research Council (MR/V002163/1). FJW is supported by a Japan Society for the Promotion of Science KAKENHI grant (JP19K16157).

Author contributions

Conceptualization: AT; Data curation: IG, IM, CB; Formal analysis: AG, CS, IG, IM; Funding acquisition: AT, MRG, MT, FJW; Investigation: AG, CS, IG, IM, FJW, MW, TJRF, MG, AB, AT; Methodology: AG, CS, IG, IM, FH, CB, AT; Project administration: AT; Resources: AB; Supervision: AT; Visualization: AG, CS, IG, IM, FJW, AT; Writing – original draft: AT; Writing – review & editing: AG, CS, IG, IM, FJW, MW, TJRF, AB, FH, CB, MRG, MT, AT.

Conflict of interest

The authors declare that they have no conflict of interest.

References

Abu-Bonsrah KD, Zhang D, Bjorksten AR, Dottori M, Newgreen DF (2018) Generation of Adrenal Chromaffin-like Cells from Human Pluripotent Stem Cells. Stem Cell Reports 10: 134-150

Agopian AJ, Bhalla AD, Boerwinkle E, Finnell RH, Grove ML, Hixson JE, Shimmin LC, Sewda A, Stuart C, Zhong Y, Zhu H, Mitchell LE (2013) Exon sequencing of PAX3 and T (brachyury) in cases with spina bifida. Birth Defects Res A Clin Mol Teratol 97: 597-601

Ahn Y, Mullan HE, Krumlauf R (2014) Long-range regulation by shared retinoic acid response elements modulates dynamic expression of posterior Hoxb genes in CNS development. Dev Biol 388: 134-44

Amemiya HM, Kundaje A, Boyle AP (2019) The ENCODE Blacklist: Identification of Problematic Regions of the Genome. Sci Rep 9: 9354

Amin S, Neijts R, Simmini S, van Rooijen C, Tan SC, Kester L, van Oudenaarden A, Creyghton MP, Deschamps J (2016) Cdx and T Brachyury Co-activate Growth Signaling in the Embryonic Axial Progenitor Niche. Cell Rep 17: 3165-3177

Anderson MJ, Schimmang T, Lewandoski M (2016) An FGF3-BMP Signaling Axis Regulates Caudal Neural Tube Closure, Neural Crest Specification and Anterior-Posterior Axis Extension. PLoS Genet 12: e1006018

Azambuja AP, Simoes-Costa M (2021) A regulatory sub-circuit downstream of Wnt signaling controls developmental transitions in neural crest formation. PLoS Genet 17: e1009296

Bardine N, Lamers G, Wacker S, Donow C, Knoechel W, Durston A (2014) Vertical signalling involves transmission of Hox information from gastrula mesoderm to neurectoderm. PLoS One 9: e115208

Beisaw A, Tsaytler P, Koch F, Schmitz SU, Melissari MT, Senft AD, Wittler L, Pennimpede T, Macura K, Herrmann BG, Grote P (2018) BRACHYURY directs histone acetylation to target loci during mesoderm development. EMBO Rep 19: 118-134

Bel-Vialar S, Itasaki N, Krumlauf R (2002) Initiating Hox gene expression: in the early chick neural tube differential sensitivity to FGF and RA signaling subdivides the HoxB genes in two distinct groups. Development 129: 5103-15

Bertero A, Pawlowski M, Ortmann D, Snijders K, Yiangou L, Cardoso de Brito M, Brown S, Bernard WG, Cooper JD, Giacomelli E, Gambardella L, Hannan NR, Iyer D, Sampaziotis F, Serrano F, Zonneveld MC, Sinha S, Kotter M, Vallier L (2016) Optimized inducible shRNA and CRISPR/Cas9 platforms for in vitro studies of human development using hPSCs. Development 143: 4405-4418

Bialecka M, Wilson V, Deschamps J (2010) Cdx mutant axial progenitor cells are rescued by grafting to a wild type environment. Dev Biol 347: 228-34

Blassberg R, Patel, H., Watson, T., Gouti, M., Metzis, V., Delas, M.J. and Briscoe, J. (2020) Sox2 levels configure the WNT response of epiblast progenitors responsible for vertebrate body formation. bioRxiv

Brend T, Gilthorpe J, Summerbell D, Rigby PW (2003) Multiple levels of transcriptional and post-transcriptional regulation are required to define the domain of Hoxb4 expression. Development 130: 2717-28

Buenrostro JD, Giresi PG, Zaba LC, Chang HY, Greenleaf WJ (2013) Transposition of native chromatin for fast and sensitive epigenomic profiling of open chromatin, DNA-binding proteins and nucleosome position. Nat Methods 10: 1213-8

Burstyn-Cohen T, Stanleigh J, Sela-Donenfeld D, Kalcheim C (2004) Canonical Wnt activity regulates trunk neural crest delamination linking BMP/noggin signaling with G1/S transition. Development 131: 5327-39

Carpenter AE, Jones TR, Lamprecht MR, Clarke C, Kang IH, Friman O, Guertin DA, Chang JH, Lindquist RA, Moffat J, Golland P, Sabatini DM (2006) CellProfiler: image analysis software for identifying and quantifying cell phenotypes. Genome Biol 7: R100

Carter TC, Pangilinan F, Troendle JF, Molloy AM, VanderMeer J, Mitchell A, Kirke PN, Conley MR, Shane B, Scott JM, Brody LC, Mills JL (2011) Evaluation of 64 candidate single nucleotide polymorphisms as risk factors for neural tube defects in a large Irish study population. Am J Med Genet A 155A: 14-21

Charite J, de Graaff W, Consten D, Reijnen MJ, Korving J, Deschamps J (1998) Transducing positional information to the Hox genes: critical interaction of cdx gene products with position-sensitive regulatory elements. Development 125: 4349-58

Chen S, Zhou Y, Chen Y, Gu J (2018) fastp: an ultra-fast all-in-one FASTQ preprocessor. Bioinformatics 34: i884-i890

Cooper F, Gentsch, G. E., Mitter, E., Bouissou, C., Healy, L., Hernandez-Rodriguez, A., Smith, J. C. and Bernardo, A. S. (2020) Rostrocaudal Patterning and Neural Crest Differentiation of Human Pre-Neural Spinal Cord Progenitors in vitro. bioRxiv

Degenhardt KR, Milewski RC, Padmanabhan A, Miller M, Singh MK, Lang D, Engleka KA, Wu M, Li J, Zhou D, Antonucci N, Li L, Epstein JA (2010) Distinct enhancers at the Pax3 locus can function redundantly to regulate neural tube and neural crest expressions. Dev Biol 339: 519-27

Delfino-Machin M, Lunn JS, Breitkreuz DN, Akai J, Storey KG (2005) Specification and maintenance of the spinal cord stem zone. Development 132: 4273-83

Denans N, Iimura T, Pourquie O (2015) Hox genes control vertebrate body elongation by collinear Wnt repression. Elife 4

Deschamps J, Duboule D (2017) Embryonic timing, axial stem cells, chromatin dynamics, and the Hox clock. Genes Dev 31: 1406-1416

Deschamps J, Wijgerde M (1993) Two phases in the establishment of HOX expression domains. Dev Biol 156: 473-80

Dias A, Lozovska A, Wymeersch FJ, Novoa A, Binagui-Casas A, Sobral D, Martins GG, Wilson V, Mallo M (2020) A Tgfbr1/Snai1-dependent developmental module at the core of vertebrate axial elongation. Elife 9

Dobin A, Davis CA, Schlesinger F, Drenkow J, Zaleski C, Jha S, Batut P, Chaisson M, Gingeras TR (2013) STAR: ultrafast universal RNA-seq aligner. Bioinformatics 29: 15-21

Dolle P, Izpisua-Belmonte JC, Falkenstein H, Renucci A, Duboule D (1989) Coordinate expression of the murine Hox-5 complex homoeobox-containing genes during limb pattern formation. Nature 342: 767-72

Dunty WC, Jr., Kennedy MW, Chalamalasetty RB, Campbell K, Yamaguchi TP (2014) Transcriptional profiling of Wnt3a mutants identifies Sp transcription factors as essential effectors of the Wnt/beta-catenin pathway in neuromesodermal stem cells. PLoS One 9: e87018

Faial T, Bernardo AS, Mendjan S, Diamanti E, Ortmann D, Gentsch GE, Mascetti VL, Trotter MW, Smith JC, Pedersen RA (2015) Brachyury and SMAD signalling collaboratively orchestrate distinct mesoderm and endoderm gene regulatory networks in differentiating human embryonic stem cells. Development 142: 2121-35

Faust GG, Hall IM (2014) SAMBLASTER: fast duplicate marking and structural variant read extraction. Bioinformatics 30: 2503-5

Faustino Martins JM, Fischer C, Urzi A, Vidal R, Kunz S, Ruffault PL, Kabuss L, Hube I, Gazzerro E, Birchmeier C, Spuler S, Sauer S, Gouti M (2020) Self-Organizing 3D Human Trunk Neuromuscular Organoids. Cell Stem Cell 26: 172-186 e6

Fellous M, Boue J, Malbrunot C, Wollman E, Sasportes M, Van Cong N, Marcelli A, Rebourcet R, Hubert C, Demenais F, Elston RC, Namboodiri KK, Kaplan EB, Fellous M (1982) A five-generation family with sacral agenesis and spina bifida: possible similarities with the mouse T-locus. Am J Med Genet 12: 465-87

Ferrer-Vaquer A, Piliszek A, Tian G, Aho RJ, Dufort D, Hadjantonakis AK (2010) A sensitive and bright single-cell resolution live imaging reporter of Wnt/ss-catenin signaling in the mouse. BMC Dev Biol 10: 121

Forlani S, Lawson KA, Deschamps J (2003) Acquisition of Hox codes during gastrulation and axial elongation in the mouse embryo. Development 130: 3807-19

Frith TJ, Granata I, Wind M, Stout E, Thompson O, Neumann K, Stavish D, Heath PR, Ortmann D, Hackland JO, Anastassiadis K, Gouti M, Briscoe J, Wilson V, Johnson SL, Placzek M, Guarracino MR, Andrews PW, Tsakiridis A (2018) Human axial progenitors generate trunk neural crest cells in vitro. Elife 7

Frith TJR, Tsakiridis A (2019) Efficient Generation of Trunk Neural Crest and Sympathetic Neurons from Human Pluripotent Stem Cells Via a Neuromesodermal Axial Progenitor Intermediate. Curr Protoc Stem Cell Biol 49: e81

Gandhi S, Hutchins EJ, Maruszko K, Park JH, Thomson M, Bronner ME (2020) Bimodal function of chromatin remodeler Hmga1 in neural crest induction and Wnt-dependent emigration. Elife 9

Gofflot F, Hall M, Morriss-Kay GM (1997) Genetic patterning of the developing mouse tail at the time of posterior neuropore closure. Dev Dyn 210: 431-45

Gomez GA, Prasad, M.S., Wong, M., Cherney, R.M., Shelar, P.B., Sandhu, N., Hackland, J.O.S., Hernandez, J.C., Leung, A.W. and Garcia, M.I. (2019) WNT/β-CATENIN modulates the axial identity of ES derived human neural crest.

Gouti M, Delile J, Stamataki D, Wymeersch FJ, Huang Y, Kleinjung J, Wilson V, Briscoe J (2017) A Gene Regulatory Network Balances Neural and Mesoderm Specification during Vertebrate Trunk Development. Dev Cell 41: 243-261 e7

Gouti M, Tsakiridis A, Wymeersch FJ, Huang Y, Kleinjung J, Wilson V, Briscoe J (2014) In vitro generation of neuromesodermal progenitors reveals distinct roles for wnt signalling in the specification of spinal cord and paraxial mesoderm identity. PLoS Biol 12: e1001937

883 Grapin-Botton A, Bonnin MA, Le Douarin NM (1997) Hox gene induction in the neural tube depends
884 on three parameters: competence, signal supply and paralogue group. Development 124: 849-59
885 Guibentif C, Griffiths JA, Imaz-Rosshandler I, Ghazanfar S, Nichols J, Wilson V, Gottgens B, Marioni JC
886 (2021) Diverse Routes toward Early Somites in the Mouse Embryo. Dev Cell 56: 141-153 e6
887 Guillot C, Djeffal Y, Michaut A, Rabe B, Pourquie O (2021) Dynamics of primitive streak regression
888 controls the fate of neuromesodermal progenitors in the chicken embryo. Elife 10
889 Hackland JOS, Frith TJR, Thompson O, Marin Navarro A, Garcia-Castro MI, Unger C, Andrews PW
890 (2017) Top-Down Inhibition of BMP Signaling Enables Robust Induction of hPSCs Into Neural Crest in
891 Fully Defined, Xeno-free Conditions. Stem Cell Reports 9: 1043-1052
892 Hackland JOS, Shelar PB, Sandhu N, Prasad MS, Charney RM, Gomez GA, Frith TJR, Garcia-Castro MI
893 (2019) FGF Modulates the Axial Identity of Trunk hPSC-Derived Neural Crest but Not the Cranial-
894 Trunk Decision. Stem Cell Reports 12: 920-933
895 Hayward AG, 2nd, Joshi P, Skromne I (2015) Spatiotemporal analysis of zebrafish hox gene regulation
896 by Cdx4. Dev Dyn 244: 1564-73
897 Heinz S, Benner C, Spann N, Bertolino E, Lin YC, Laslo P, Cheng JX, Murre C, Singh H, Glass CK (2010)
898 Simple combinations of lineage-determining transcription factors prime cis-regulatory elements
899 required for macrophage and B cell identities. Mol Cell 38: 576-89
900 Henrique D, Abranches E, Verrier L, Storey KG (2015) Neuromesodermal progenitors and the making
901 of the spinal cord. Development 142: 2864-75
902 Huang SM, Mishina YM, Liu S, Cheung A, Stegmeier F, Michaud GA, Charlat O, Wiellette E, Zhang Y,
903 Wiessner S, Hild M, Shi X, Wilson CJ, Mickanin C, Myer V, Fazal A, Tomlinson R, Serluca F, Shao W,
904 Cheng H et al. (2009) Tankyrase inhibition stabilizes axin and antagonizes Wnt signalling. Nature 461:
905 614-20
906 Izpisua-Belmonte JC, Falkenstein H, Dolle P, Renucci A, Duboule D (1991) Murine genes related to
907 the Drosophila AbdB homeotic genes are sequentially expressed during development of the
908 posterior part of the body. EMBO J 10: 2279-89
909 Javali A, Misra A, Leonavicius K, Acharyya D, Vyas B, Sambasivan R (2017) Co-expression of Tbx6 and
910 Sox2 identifies a novel transient neuromesoderm progenitor cell state. Development 144: 4522-4529
911 Kirino K, Nakahata T, Taguchi T, Saito MK (2018) Efficient derivation of sympathetic neurons from
912 human pluripotent stem cells with a defined condition. Sci Rep 8: 12865
913 Koch F, Scholze M, Wittler L, Schifferl D, Sudheer S, Grote P, Timmermann B, Macura K, Herrmann
914 BG (2017) Antagonistic Activities of Sox2 and Brachyury Control the Fate Choice of Neuro-
915 Mesodermal Progenitors. Dev Cell 42: 514-526 e7
916 Langmead B, Salzberg SL (2012) Fast gapped-read alignment with Bowtie 2. Nat Methods 9: 357-9
917 Le Douarin NM, Creuzet S, Couly G, Dupin E (2004) Neural crest cell plasticity and its limits.
918 Development 131: 4637-50
919 Leung AW, Murdoch B, Salem AF, Prasad MS, Gomez GA, Garcia-Castro MI (2016) WNT/beta-catenin
920 signaling mediates human neural crest induction via a pre-neural border intermediate. Development
921 143: 398-410
922 Li B, Dewey CN (2011) RSEM: accurate transcript quantification from RNA-Seq data with or without a
923 reference genome. BMC Bioinformatics 12: 323
924 Li H, Durbin R (2009) Fast and accurate short read alignment with Burrows-Wheeler transform.
925 Bioinformatics 25: 1754-60
926 Libby ARG, Joy DA, Elder NH, Bulger EA, Krakora MZ, Gaylord EA, Mendoza-Camacho F, Butts JC,
927 McDevitt TC (2021) Axial elongation of caudalized human organoids mimics aspects of neural tube
928 development. Development 148
929 Lippmann ES, Williams CE, Ruhl DA, Estevez-Silva MC, Chapman ER, Coon JJ, Ashton RS (2015)
930 Deterministic HOX patterning in human pluripotent stem cell-derived neuroectoderm. Stem Cell
931 Reports 4: 632-44

Liu JA, Wu MH, Yan CH, Chau BK, So H, Ng A, Chan A, Cheah KS, Briscoe J, Cheung M (2013) Phosphorylation of Sox9 is required for neural crest delamination and is regulated downstream of BMP and canonical Wnt signaling. Proc Natl Acad Sci U S A 110: 2882-7

Liu JP, Laufer E, Jessell TM (2001) Assigning the positional identity of spinal motor neurons: rostrocaudal patterning of Hox-c expression by FGFs, Gdf11, and retinoids. Neuron 32: 997-1012

Lolas M, Valenzuela PD, Tjian R, Liu Z (2014) Charting Brachyury-mediated developmental pathways during early mouse embryogenesis. Proc Natl Acad Sci U S A 111: 4478-83

Lopez-Yrigoyen M, Fidanza A, Cassetta L, Axton RA, Taylor AH, Meseguer-Ripolles J, Tsakiridis A, Wilson V, Hay DC, Pollard JW, Forrester LM (2018) A human iPSC line capable of differentiating into functional macrophages expressing ZsGreen: a tool for the study and in vivo tracking of therapeutic cells. Philos Trans R Soc Lond B Biol Sci 373

Love MI, Huber W, Anders S (2014) Moderated estimation of fold change and dispersion for RNA-seq data with DESeq2. Genome Biol 15: 550

Lukoseviciute M, Mayes, S. and Sauka-Spengler, T. (2021) Neuromesodermal progenitor origin of trunk neural crest in vivo. bioRxiv

Mariani L, Guo X, Menezes NA, Drozd AM, Cakal SD, Wang Q, Ferretti E (2021) A TALE/HOX code unlocks WNT signalling response towards paraxial mesoderm. Nat Commun 12: 5136

Martin BL, Kimelman D (2010) Brachyury establishes the embryonic mesodermal progenitor niche. Genes Dev 24: 2778-83

Martin BL, Kimelman D (2012) Canonical Wnt signaling dynamically controls multiple stem cell fate decisions during vertebrate body formation. Dev Cell 22: 223-32

Mazzoni EO, Mahony S, Peljto M, Patel T, Thornton SR, McCuine S, Reeder C, Boyer LA, Young RA, Gifford DK, Wichterle H (2013) Saltatory remodeling of Hox chromatin in response to rostrocaudal patterning signals. Nat Neurosci 16: 1191-1198

McGrew MJ, Sherman A, Lillico SG, Ellard FM, Radcliffe PA, Gilhooley HJ, Mitrophanous KA, Cambray N, Wilson V, Sang H (2008) Localised axial progenitor cell populations in the avian tail bud are not committed to a posterior Hox identity. Development 135: 2289-99

Metzis V, Steinhauser S, Pakanavicius E, Gouti M, Stamataki D, Ivanovitch K, Watson T, Rayon T, Mousavy Gharavy SN, Lovell-Badge R, Luscombe NM, Briscoe J (2018) Nervous System Regionalization Entails Axial Allocation before Neural Differentiation. Cell 175: 1105-1118 e17

Mitchell PJ, Timmons PM, Hebert JM, Rigby PW, Tjian R (1991) Transcription factor AP-2 is expressed in neural crest cell lineages during mouse embryogenesis. Genes Dev 5: 105-19

Morrison K, Papapetrou C, Attwood J, Hol F, Lynch SA, Sampath A, Hamel B, Burn J, Sowden J, Stott D, Mariman E, Edwards YH (1996) Genetic mapping of the human homologue (T) of mouse T(Brachyury) and a search for allele association between human T and spina bifida. Hum Mol Genet 5: 669-74

Mouilleau V, Vaslin C, Robert R, Gribaudo S, Nicolas N, Jarrige M, Terray A, Lesueur L, Mathis MW, Croft G, Daynac M, Rouiller-Fabre V, Wichterle H, Ribes V, Martinat C, Nedelec S (2021) Dynamic extrinsic pacing of the HOX clock in human axial progenitors controls motor neuron subtype specification. Development 148

Muhr J, Graziano E, Wilson S, Jessell TM, Edlund T (1999) Convergent inductive signals specify midbrain, hindbrain, and spinal cord identity in gastrula stage chick embryos. Neuron 23: 689-702

Neijts R, Amin S, van Rooijen C, Deschamps J (2017) Cdx is crucial for the timing mechanism driving colinear Hox activation and defines a trunk segment in the Hox cluster topology. Dev Biol 422: 146-154

Neijts R, Amin S, van Rooijen C, Tan S, Creyghton MP, de Laat W, Deschamps J (2016) Polarized regulatory landscape and Wnt responsiveness underlie Hox activation in embryos. Genes Dev 30: 1937-42

Nordstrom U, Maier E, Jessell TM, Edlund T (2006) An early role for WNT signaling in specifying neural patterns of Cdx and Hox gene expression and motor neuron subtype identity. PLoS Biol 4: e252

983 Nowotschin S, Ferrer-Vaquer A, Hadjantonakis AK (2010) Imaging mouse development with confocal
984 time-lapse microscopy. Methods Enzymol 476: 351-77
985 Olivera-Martinez I, Harada H, Halley PA, Storey KG (2012) Loss of FGF-dependent mesoderm identity
986 and rise of endogenous retinoid signalling determine cessation of body axis elongation. PLoS Biol 10:
987 e1001415
988 Olivera-Martinez I, Schurch N, Li RA, Song J, Halley PA, Das RM, Burt DW, Barton GJ, Storey KG (2014)
989 Major transcriptome re-organisation and abrupt changes in signalling, cell cycle and chromatin
990 regulation at neural differentiation in vivo. Development 141: 3266-76
991 Pilon N (2021) Treatment and Prevention of Neurocristopathies. Trends Mol Med 27: 451-468
992 Poncet N, Halley PA, Lipina C, Gierlinski M, Dady A, Singer GA, Febrer M, Shi YB, Yamaguchi TP,
993 Taylor PM, Storey KG (2020) Wnt regulates amino acid transporter Slc7a5 and so constrains the
994 integrated stress response in mouse embryos. EMBO Rep 21: e48469
995 Rashbass P, Cooke LA, Herrmann BG, Beddington RS (1991) A cell autonomous function of Brachyury
996 in T/T embryonic stem cell chimaeras. Nature 353: 348-51
997 Rocha M, Beiriger A, Kushkowski EE, Miyashita T, Singh N, Venkataraman V, Prince VE (2020) From
998 head to tail: regionalization of the neural crest. Development 147
999 Rochtus A, Izzi B, Vangeel E, Louwette S, Wittevrongel C, Lambrechts D, Moreau Y, Winand R,
1000 Verpoorten C, Jansen K, Van Geet C, Freson K (2015) DNA methylation analysis of Homeobox genes
1001 implicates HOXB7 hypomethylation as risk factor for neural tube defects. Epigenetics 10: 92-101
1002 Rodrigo Albors A, Halley PA, Storey KG (2018) Lineage tracing of axial progenitors using Nkx1-
1003 2CreER(T2) mice defines their trunk and tail contributions. Development 145
1004 Rothstein M, Bhattacharya D, Simoes-Costa M (2018) The molecular basis of neural crest axial
1005 identity. Dev Biol 444 Suppl 1: S170-S180
1006 Rothstein M, Simoes-Costa M (2020) Heterodimerization of TFAP2 pioneer factors drives epigenomic
1007 remodeling during neural crest specification. Genome Res 30: 35-48
1008 Sanchez-Ferras O, Bernas G, Farnos O, Toure AM, Souchkova O, Pilon N (2016) A direct role for
1009 murine Cdx proteins in the trunk neural crest gene regulatory network. Development 143: 1363-74
1010 Sanchez-Ferras O, Bernas G, Laberge-Perrault E, Pilon N (2014) Induction and dorsal restriction of
1011 Paired-box 3 (Pax3) gene expression in the caudal neuroectoderm is mediated by integration of
1012 multiple pathways on a short neural crest enhancer. Biochim Biophys Acta 1839: 546-58
1013 Sanchez-Ferras O, Coutaud B, Djavanbakht Samani T, Tremblay I, Souchkova O, Pilon N (2012)
1014 Caudal-related homeobox (Cdx) protein-dependent integration of canonical Wnt signaling on paired-
1015 box 3 (Pax3) neural crest enhancer. J Biol Chem 287: 16623-35
1016 Schindelin J, Arganda-Carreras I, Frise E, Kaynig V, Longair M, Pietzsch T, Preibisch S, Rueden C,
1017 Saalfeld S, Schmid B, Tinevez JY, White DJ, Hartenstein V, Eliceiri K, Tomancak P, Cardona A (2012)
1018 Fiji: an open-source platform for biological-image analysis. Nat Methods 9: 676-82
1019 Shaker MR, Lee JH, Kim KH, Ban S, Kim VJ, Kim JY, Lee JY, Sun W (2021) Spatiotemporal contribution
1020 of neuromesodermal progenitor-derived neural cells in the elongation of developing mouse spinal
1021 cord. Life Sci: 119393
1022 Shields DC, Ramsbottom D, Donoghue C, Pinjon E, Kirke PN, Molloy AM, Edwards YH, Mills JL,
1023 Mynett-Johnson L, Weir DG, Scott JM, Whitehead AS (2000) Association between historically high
1024 frequencies of neural tube defects and the human T homologue of mouse T (Brachyury). Am J Med
1025 Genet 92: 206-11
1026 Simoes-Costa M, Bronner ME (2016) Reprogramming of avian neural crest axial identity and cell fate.
1027 Science 352: 1570-3
1028 Stavish D, Boiers C, Price C, Frith TJR, Halliwell J, Saldana-Guerrero I, Wray J, Brown J, Carr J, James C,
1029 Barbaric I, Andrews PW, Enver T (2020) Generation and trapping of a mesoderm biased state of
1030 human pluripotency. Nat Commun 11: 4989
1031 Takemoto T, Abe T, Kiyonari H, Nakao K, Furuta Y, Suzuki H, Takada S, Fujimori T, Kondoh H (2016)
1032 R26-WntVis reporter mice showing graded response to Wnt signal levels. Genes Cells 21: 661-9

1033 Takemoto T, Uchikawa M, Kamachi Y, Kondoh H (2006) Convergence of Wnt and FGF signals in the
1034 genesis of posterior neural plate through activation of the Sox2 enhancer N-1. Development 133:
1035 297-306
1036 Tao YX, Rumbaugh G, Wang GD, Petralia RS, Zhao C, Kauer FW, Tao F, Zhuo M, Wenthold RJ, Raja SN,
1037 Huganir RL, Bredt DS, Johns RA (2003) Impaired NMDA receptor-mediated postsynaptic function and
1038 blunted NMDA receptor-dependent persistent pain in mice lacking postsynaptic density-93 protein. J
1039 Neurosci 23: 6703-12
1040 Thomson JA, Itskovitz-Eldor J, Shapiro SS, Waknitz MA, Swiergiel JJ, Marshall VS, Jones JM (1998)
1041 Embryonic stem cell lines derived from human blastocysts. Science 282: 1145-7
1042 Tosic J, Kim GJ, Pavlovic M, Schroder CM, Mersiowsky SL, Barg M, Hofherr A, Probst S, Kottgen M,
1043 Hein L, Arnold SJ (2019) Eomes and Brachyury control pluripotency exit and germ-layer segregation
1044 by changing the chromatin state. Nat Cell Biol 21: 1518-1531
1045 Tsakiridis A, Huang Y, Blin G, Skylaki S, Wymeersch F, Osorno R, Economou C, Karagianni E, Zhao S,
1046 Lowell S, Wilson V (2014) Distinct Wnt-driven primitive streak-like populations reflect in vivo lineage
1047 precursors. Development 141: 1209-21
1048 Tzouanacou E, Wegener A, Wymeersch FJ, Wilson V, Nicolas JF (2009) Redefining the progression of
1049 lineage segregations during mammalian embryogenesis by clonal analysis. Dev Cell 17: 365-76
1050 van de Ven C, Bialecka M, Neijts R, Young T, Rowland JE, Stringer EJ, Van Rooijen C, Meijlink F, Novoa
1051 A, Freund JN, Mallo M, Beck F, Deschamps J (2011) Concerted involvement of Cdx/Hox genes and
1052 Wnt signaling in morphogenesis of the caudal neural tube and cloacal derivatives from the posterior
1053 growth zone. Development 138: 3451-62
1054 van den Akker E, Fromental-Ramain C, de Graaff W, Le Mouellic H, Brulet P, Chambon P, Deschamps
1055 J (2001) Axial skeletal patterning in mice lacking all paralogous group 8 Hox genes. Development
1056 128: 1911-21
1057 van Rooijen C, Simmini S, Bialecka M, Neijts R, van de Ven C, Beck F, Deschamps J (2012)
1058 Evolutionarily conserved requirement of Cdx for post-occipital tissue emergence. Development 139:
1059 2576-83
1060 Vega-Lopez GA, Cerrizuela S, Tribulo C, Aybar MJ (2018) Neurocristopathies: New insights 150 years
1061 after the neural crest discovery. Dev Biol 444 Suppl 1: S110-S143
1062 Wacker SA, McNulty CL, Durston AJ (2004) The initiation of Hox gene expression in Xenopus laevis is
1063 controlled by Brachyury and BMP-4. Dev Biol 266: 123-37
1064 Wind M, Gogolou A, Manipur I, Granata I, Butler L, Andrews PW, Barbaric I, Ning K, Guarracino MR,
1065 Placzek M, Tsakiridis A (2021) Defining the signalling determinants of a posterior ventral spinal cord
1066 identity in human neuromesodermal progenitor derivatives. Development 148
1067 Wood HB, Episkopou V (1999) Comparative expression of the mouse Sox1, Sox2 and Sox3 genes
1068 from pre-gastrulation to early somite stages. Mech Dev 86: 197-201
1069 Wymeersch FJ, Huang Y, Blin G, Cambray N, Wilkie R, Wong FC, Wilson V (2016) Position-dependent
1070 plasticity of distinct progenitor types in the primitive streak. Elife 5: e10042
1071 Wymeersch FJ, Skylaki S, Huang Y, Watson JA, Economou C, Marek-Johnston C, Tomlinson SR, Wilson
1072 V (2019) Transcriptionally dynamic progenitor populations organised around a stable niche drive
1073 axial patterning. Development 146
1074 Wymeersch FJ, Wilson V, Tsakiridis A (2021) Understanding axial progenitor biology in vivo and in
1075 vitro. Development 148
1076 Ye Z, Braden CR, Wills A, Kimelman D (2021) Identification of in vivo Hox13-binding sites reveals an
1077 essential locus controlling zebrafish brachyury expression. Development 148
1078 Ye Z, Kimelman D (2020) Hox13 genes are required for mesoderm formation and axis elongation
1079 during early zebrafish development. Development 147
1080 Young T, Rowland JE, van de Ven C, Bialecka M, Novoa A, Carapuco M, van Nes J, de Graaff W, Duluc
1081 I, Freund JN, Beck F, Mallo M, Deschamps J (2009) Cdx and Hox genes differentially regulate
1082 posterior axial growth in mammalian embryos. Dev Cell 17: 516-26

Yu J, Wang L, Pei P, Li X, Wu J, Qiu Z, Zhang J, Ao R, Wang S, Zhang T, Xie J (2019) Reduced H3K27me3 leads to abnormal Hox gene expression in neural tube defects. Epigenetics Chromatin 12: 76

Zhang Y, Liu T, Meyer CA, Eeckhoute J, Johnson DS, Bernstein BE, Nusbaum C, Myers RM, Brown M, Li W, Liu XS (2008) Model-based analysis of ChIP-Seq (MACS). Genome Biol 9: R137

Zhao T, Gan Q, Stokes A, Lassiter RN, Wang Y, Chan J, Han JX, Pleasure DE, Epstein JA, Zhou CJ (2014) beta-catenin regulates Pax3 and Cdx2 for caudal neural tube closure and elongation. Development 141: 148-57

Figure legends

Figure 1. Effect of TBXT reduction on hPSC-derived NMPs. (A) Differentiation/treatment scheme. **(B)** Immunofluorescence analysis of the expression of TBXT in shRNA hESC-derived NMPs in the presence and absence of tetracycline (Tet). **(C)** Mean fluorescence intensity of TBXT protein in Tet-treated and control NMP cultures. **(D)** Normalised expression values of TBXT transcripts in control, Tet-treated NMPs and undifferentiated hES cell samples following RNA-seq analysis. **(E)** GO term analysis of differentially expressed genes in hESC-derived NMPs following TBXT knockdown. **(F)** Representative significantly down- and upregulated transcripts following TBXT depletion. **(G)** qPCR expression analysis of indicated HOX genes in control vs Tet-treated NMPs.

Figure 2. TBXT depletion impairs posterior axial identity acquisition by neural crest. **(A)** Differentiation/treatment scheme. **(B)** qPCR expression analysis of indicated HOX genes in control vs Tet-treated NMP-derived trunk neural crest cells**. (C)** Immunofluorescence analysis of the expression of HOXC9 in control vs Tet-treated NMP-derived trunk neural crest cells. Quantification of $HOXC9^{+}$ cells in the presence and absence of Tet is also shown. **(D)** qPCR expression analysis of indicated markers in control vs Tet-treated NMP-derived trunk neural crest cells. **(E)** Immunofluorescence analysis of the expression of SOX10 in control vs Tet-treated NMP-derived trunk neural crest cells. Quantification of $SOX10^{+}$ cells in the presence and absence of Tet is also shown. NC, neural crest. *P<0.05, **P<0.01, n.s. not significant (Paired t-test).

Figure 3. Early programming of a posterior axial identity in NMP-derived neural crest cells is primarily WNT-dependent.
(A) Scheme of treatments during the differentiation of hPSCs toward NMPs. **(B)** qPCR expression analysis of representative WNT-FGF targets in NMP cultures treated with the indicated combinations of WNT-FGF agonists/antagonists. **(C-D)** qPCR expression analysis of key NMP markers **(C)** and HOX genes **(D)** in NMP cultures treated with the indicated combinations of WNT-FGF agonists/antagonists. **(E)** Scheme of treatments during the

differentiation of hPSC-derived NMPs toward trunk neural crest (NC) cells. **(G-F)** qPCR expression analysis of representative lineage-specific, axial identity **(G)** and HOX genes **(F)** in NMP-derived trunk NC cultures treated with the indicated combinations of WNT-BMP agonists/antagonists.

Figure 4. Wnt signalling dynamics during posterior neural crest emergence. **(A)** Fluorescence microscopy analysis of R26-WntVis mouse embryos at E8.75 (Theiler Stage; TS13) and E9.0 (TS14) showing graded responsiveness to Wnt signalling in the posterior growth region. **(B)** Sagittal sections of immunostained *R26-WntVis* tail buds showing a-GFP signal in the T^+ lateral-most caudal epiblast (LE; dashed lines) at E8.75 (**Ba-c**) and E9.0 (**Bd-f**). Arrowheads indicate T^- surface ectoderm cells. (**Bg-j**) 3D reconstruction and processing of imaging data showing T^+ volumes overlapping with a-GFP^{high} volumes (i.e. Wnt^{high} T^+ cells) in the LE: posterior view at E8.75 (**Bg-h**) and lateral view at E9.0 (**Bi-j**). A cut-off was made to show only higher expressing a-GFP^+ volumes (see **EV2**). Nuclei were defined by anti-Laminin B1 staining (LB1). **(C)** Wholemount immunostaining and corresponding 3D analysis showing NC derivatives and their progenitors at different sections of the rostrocaudal axis (regions corresponding to blue boxes in A). Insets corresponding to the dash line-boxed areas show the a-GFP and overlaid Sox9 and Tfap2a channels, respectively. (**Ca-b, Cg-i**) $Sox9^+$ $Tfap2a^+$ cells in the developing head mesenchyme. $Sox9^+$ $Tfap2a^+$ NC cells emerging from the E8.75 dorsal neural tube show low Wnt activity (**Cc-d**), whereas those at E9.0 generally exhibit a higher GFP signal (compare Cc to Cj). Asterisks mark dorsal somite cells. At E8.75, no $Tfap2a^+GFP^+$ cells were observed in the LE layer (**Ce-f**), whereas at E9.0 the caudalmost epiblast contains a population of $Tfap2a^+$ GFP^+ cells (arrows in Cm-o). HF, headfolds; HM, head mesenchyme; NCC, neural crest cells; Noto, notochord; NT, neural tube; PS, primitive streak; Som, somite; SE, surface ectoderm; TG, tail gut; A, anterior; P, posterior; D, dorsal; V, ventral; L, left; R, right. Scale bars=50 µm.

Figure 5. TBXT controls the HOX clock and WNT signalling in NMPs by influencing chromatin accessibility. (A) Representative transcription factor-binding motifs enriched in TBXT binding sites. **(B)** Graph showing the percentages of differentially expressed genes (Padj<0.05, log2FC> |1|) following TBXT knockdown during the transition of hESCs toward NMPs that are bound directly by TBXT. **(C)** Table showing all differentially expressed genes following TBXT knockdown that exhibit TBXT binding within their promoter region. **(D)** Volcano plot of differentially accessible ATAC seq peaks between TBXT-depleted and control NMPs. **(E)** Graph showing the number of significantly up- and down-regulated direct TBXT targets in relation to changes in chromatin accessibility associated with TBXT knockdown. **(F)** Correspondence between TBXT binding (ChiP) and chromatin accessibility

changes (ATAC-seq) in the presence and absence of Tet in indicated HOX clusters, WNT/presomitic mesoderm-linked loci. **(G)** Correspondence between TBXT binding and chromatin accessibility changes in the presence and absence of Tet in indicated neural differentiation-linked loci.

Figure 6. Posterior axial identity acquisition by NMP-derived pre-neural spinal cord cells is TBXT-independent. (A, D) Differentiation/treatment schemes associated with different time windows of TBXT knockdown during spinal cord differentiation from NMPs. **(B-C, E-F)** qPCR expression analysis of indicated HOX genes (**B, E**) and representative NMP/early spinal cord markers (**C, F**) in control vs Tet-treated NMP-derived early spinal cord progenitors corresponding to the Tet treatment regimens shown in A and D respectively.

Figure 7. Posterior axial identity acquisition by NMP-derived spinal cord progenitors is FGF-dependent. (A) Scheme of treatments during the differentiation of hPSC-derived NMPs toward early spinal cord progenitors. **(B-C)** qPCR expression analysis of indicated HOX genes **(B)** and representative NMP/early spinal cord/neural markers **(C)** in NMP-derived early spinal cord cultures treated with the indicated combinations of WNT-FGF agonists/antagonists as depicted in A. **(D)** Immunofluorescence analysis of CDX2 and HOXC9 protein expression in NMP-derived early spinal cord cultures treated with the indicated combinations of WNT-FGF agonists/antagonists. **(E)** Proposed model for the transcriptional and signalling control of posterior axial identity/Hox clock in hPSC-derived NMPs and their derivatives.

Tables and their legends

Appendix Table S1. Significantly up- and downregulated transcripts in Tet-treated, TBXT-depleted hESC-derived NMPs.

Appendix Table S2. List of GO terms and corresponding gene lists enriched in Tet-treated, TBXT depleted hESC-derived NMPs

Appendix Table S3. List of all genomic regions (Intervals) with peak p-value below the applied threshold bound by TBXT in hESC-derived NMPs and undifferentiated hESCs.

Appendix Table S4. List of GO terms and corresponding gene lists associated with TBXT binding sites in hPSC-derived NMPs.

Appendix Table S5. List of known HOMER database motifs enriched in TBXT binding sites in hESC-derived NMPs.

Appendix Table S6. List of TBXT target genes which are differentially expressed following Tet treatment (P adj <0.05 log2FC > |0.5|) and Gene Ontology Biological Processes

enrichment analysis. Genes are listed in relation to the genomic position (in relation to TSS) of TBXT binding within their proximity. Blue highlight denotes downregulation while red represents upregulation in expression.

Appendix Table S7. List of ATAC-seq peaks associated with gain or loss of chromatin accessibility following TBXT depletion in hESC-derived NMPs. Gene Ontology Biological Processes enrichment analysis, list of HOX genes as well as other genes (P adj <0.05 log2FC > |1|) affected by TBXT depletion and are associated with changes in chromatin accessibility are also included.

Appendix Table S8. List of transcription factor DNA binding motifs enriched in ATAC-seq sites associated with chromatin accessibility gain, chromatin accessibility loss or both.

Appendix Table S9. List of primers used.

Expanded View Figure legends

Figure EV1. Effect of tetracycline treatment on control B2M shRNA hESC-derived NMPs. (A) Immunofluorescence analysis of the expression of TBXT in control B2M shRNA hESC-derived NMPs in the presence and absence of tetracycline (Tet). **(B)** qPCR expression analysis of indicated HOX genes in control vs Tet-treated NMPs generated from B2M shRNA hESCs.

Figure EV2. Wnt signalling dynamics during posterior neural crest emergence. Top: Schematics showing location and orientation of immunostaining data in E8.75 (TS13) and E9.0 (TS14) embryos. **(A)** Confocal sections of wholemount immunostaining shows graded responsiveness to Wnt signalling in T^+ lateral-most caudal epiblast (LE, indicated by dashed lines). (**B-C**) Additional 3D views to *R26-WntVis* tail buds shown in **Fig.4B**: wholemount a-GFP staining (**Ba, Ca**), cut-off and mean intensity of GFP^{high} volumes (3D vol) (**Bb, Cb**) and overlap of Wnt^{high} and T^+ volumes in the LE (dashed lines; **Bc, Cc**). The colour scale shows mean pixel intensity of a-GFP^{high} volumes, their numbers denoting the outermost values. **(D)** Comparison between a-GFP wholemount immunostaining data (magenta) to a-GFP^{high} 3D volume calculation (pink) and their mean pixel intensity (fire scale). (**Da-c)** Frontal view of the head region: a-GFP^{low} cells can be seen in the headfolds (HF; dotted lines) but were largely excluded from the analysis (arrowheads). **(Dd-f)** Dorsal view on the neural tube (NT, dotted lines). **(Dg-l, Dp-r)** Lateral view of the tail bud showing the LE (dotted lines). **(Dj-l)** Lateral view of the E9.0 head mesenchyme shows a-GFP^{low} cells are present in the hindbrain (HB, dotted lines). Note the gradient in a-GFP^+ in neural crest cells (NCC; **Dl**). **(Dm-o)** E9.0 posterior axis shows high reporter expression in dorsal somites, graded from anterior to posterior (asterisks). Noto, notochord; PS, primitive streak;

PSM, presomitic mesoderm; Som, somite; SE, surface ectoderm; TG, tail gut; A, anterior; P, posterior; D, dorsal; V, ventral; L, left; R, right. Scale bars=50 µm.

Figure EV3. Effect of TBXT binding on chromatin accessibility. (A) Average density plot of tag distributions across peak regions corresponding to the NMP, hES and input samples. **(B)** Genomic distribution of TBXT-bound sites in hPSC-derived NMPs. **(C)** Gene ontology biological processes enrichment analysis of target genes associated with TXBT binding sites around their transcriptional start site (-2000 to +500 bp). **(D)** Correspondence between TBXT binding (ChiP) and chromatin accessibility changes (ATAC-seq) in the presence and absence of Tet in indicated HOX and WNT-linked loci. **(E)** Venn diagram showing the overalp between transcription factor DNA binding motifs in genomic regions associated with chromatin accessibility gain and loss following TBXT knockdown.

Gogolou et al_Figure 1

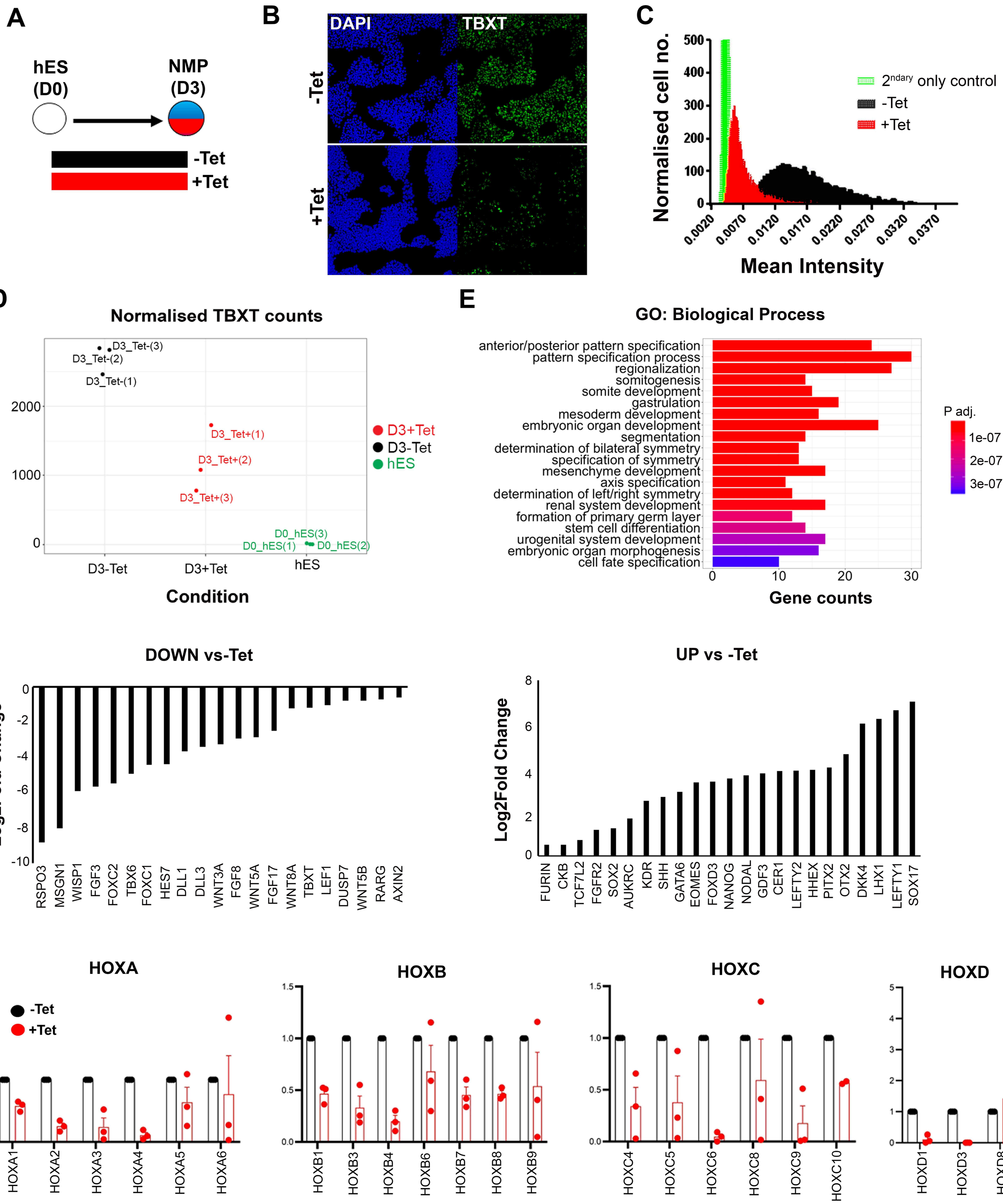

Figure 1. Effect of TBXT reduction on hPSC-derived NMPs. (A) Differentiation/treatment scheme. **(B)** Immunofluorescence analysis of the expression of TBXT in shRNA hESC-derived NMPs in the presence and absence of tetracycline (Tet). **(C)** Mean fluorescence intensity of TBXT protein in Tet-treated and control NMP cultures. **(D)** Normalised expression values of TBXT transcripts in control, Tet-treated NMPs and undifferentiated hES cell samples following RNA-seq analysis. **(E)** GO term analysis of differentially expressed genes in hESC-derived NMPs following TBXT knockdown **(F)** Representative significantly down- and upregulated transcripts following TBXT depletion. **(G)** qPCR expression analysis of indicated HOX genes in control vs Tet-treated NMPs.

Gogolou et al_Figure 2

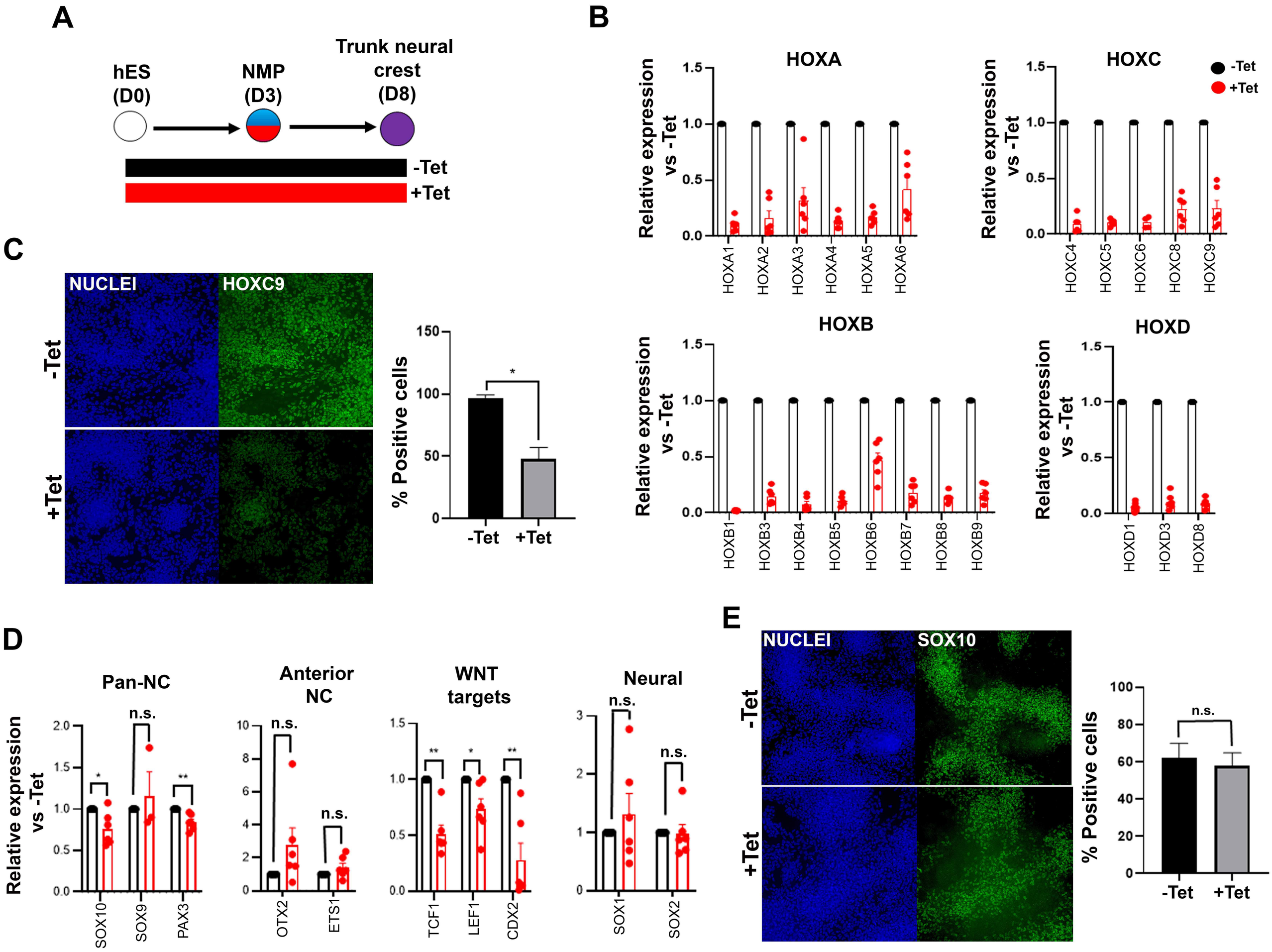

Figure 2. TBXT depletion impairs posterior axial identity acquisition by neural crest. (A) Differentiation/treatment scheme. **(B)** qPCR expression analysis of indicated HOX genes in control vs Tet-treated NMP-derived trunk neural crest cells. **(C)** Immunofluorescence analysis of the expression of HOXC9 in control vs Tet-treated NMP-derived trunk neural crest cells. Quantification of HOXC9$^+$ cells in the presence and absence of Tet is also shown. **(D)** qPCR expression analysis of indicated markers in control vs Tet-treated NMP-derived trunk neural crest cells. **(E)** Immunofluorescence analysis of the expression of SOX10 in control vs Tet-treated NMP-derived trunk neural crest cells. Quantification of SOX10$^+$ cells in the presence and absence of Tet is also shown. NC, neural crest. *P<0.05, **P<0.01, n.s. not significant (Paired t-test).

Gogolou et al_Figure 3

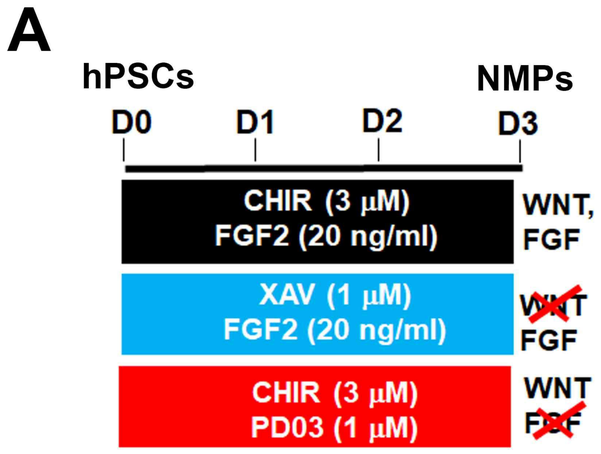

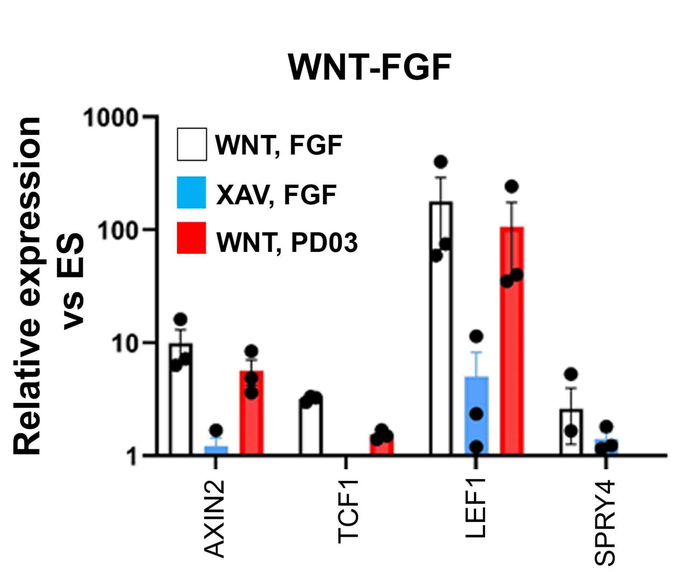

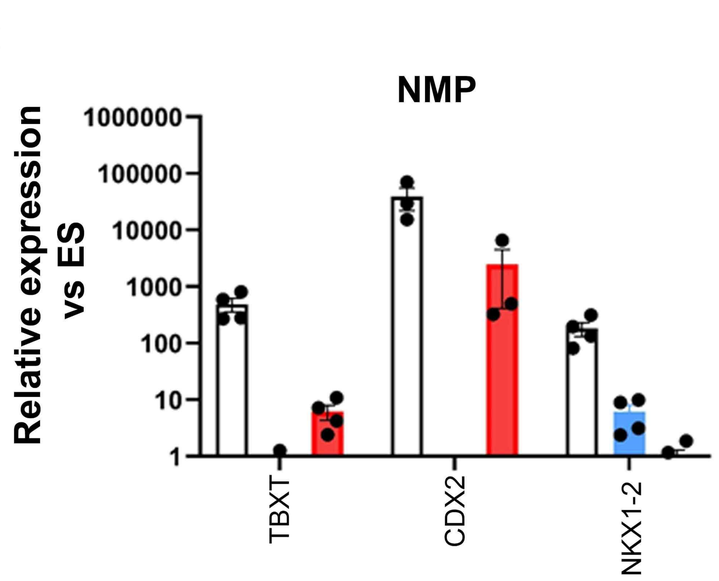

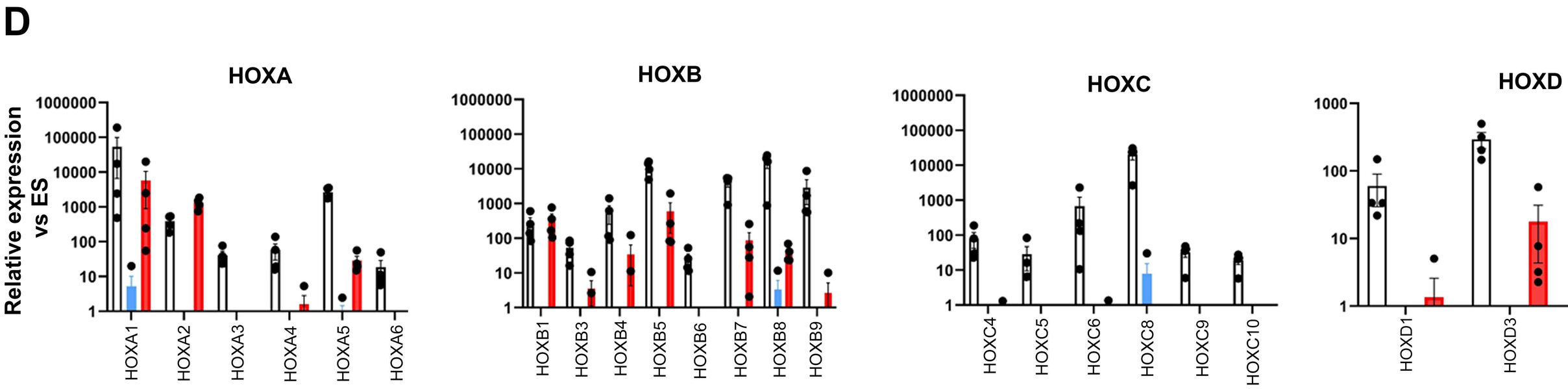

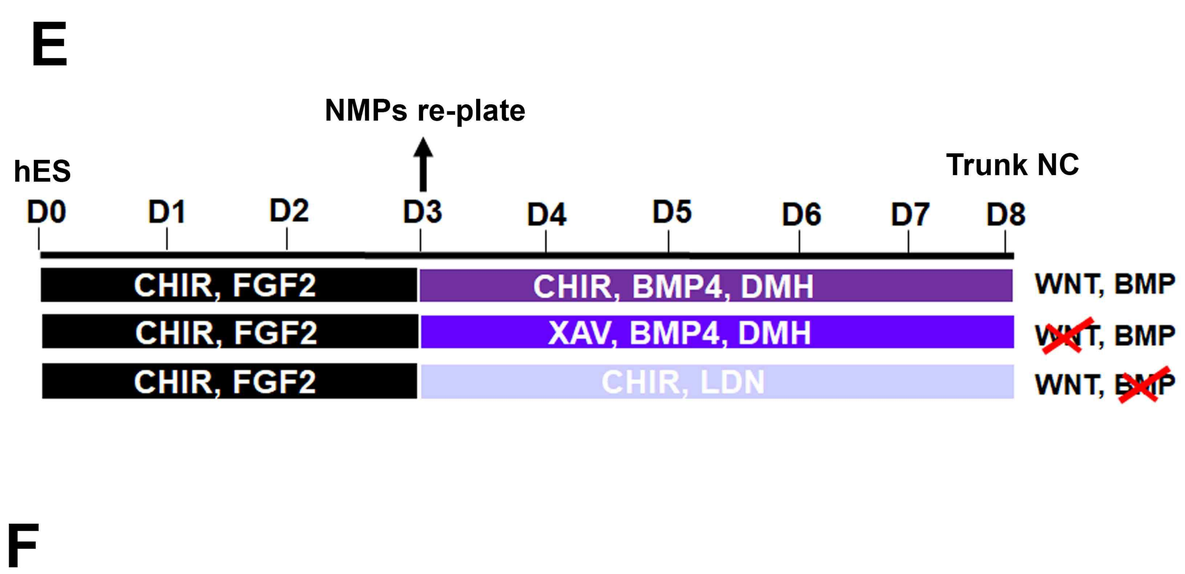

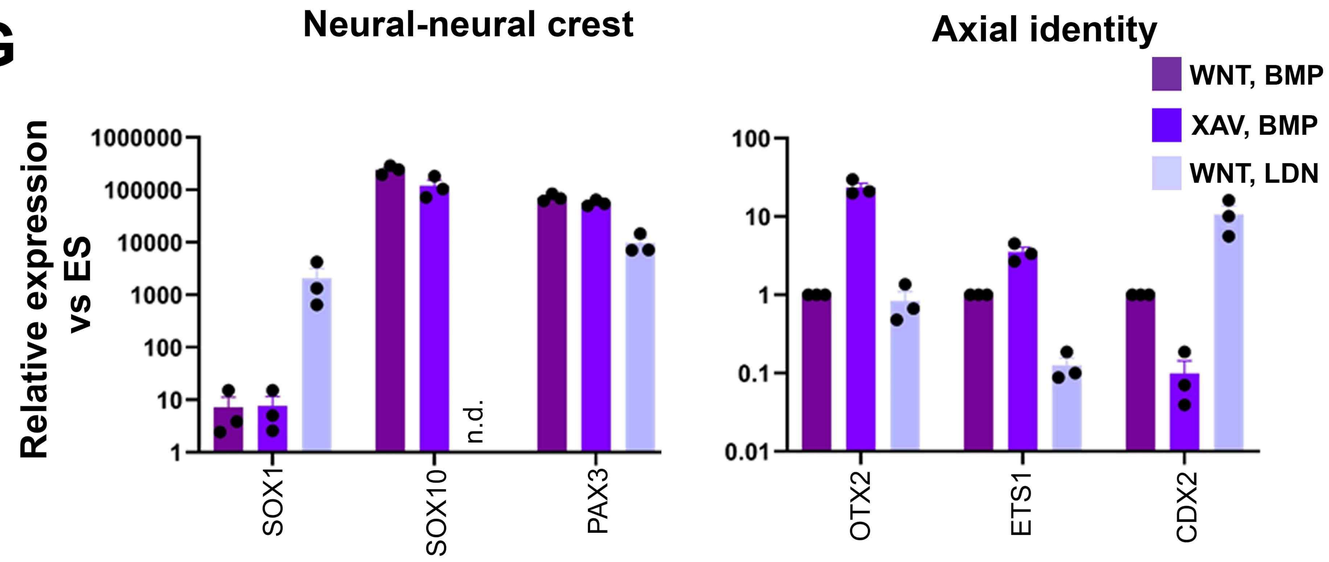

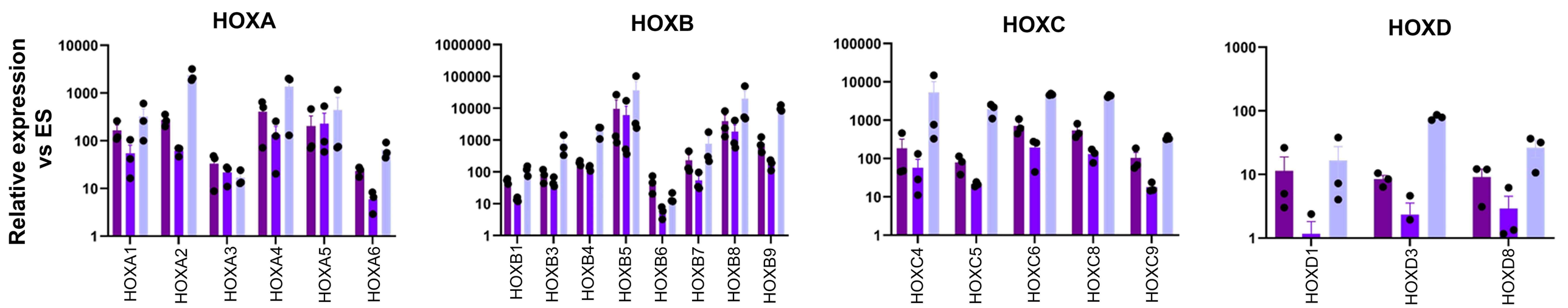

Figure 3. Early programming of a posterior axial identity in NMP-derived neural crest cells is primarily WNT-dependent. **(A)** Scheme of treatments during the differentiation of hPSCs toward NMPs. **(B)** qPCR expression analysis of representative WNT-FGF targets in NMP cultures treated with the indicated combinations of WNT-FGF agonists/antagonists. **(C-D)** qPCR expression analysis of key NMP markers **(C)** and HOX genes **(D)** in NMP cultures treated with the indicated combinations of WNT-FGF agonists/antagonists.**(E)** Scheme of treatments during the differentiation of hPSC-derived NMPs toward trunk neural crest (NC) cells. **(G-F)** qPCR expression analysis of representative lineage-specific, axial identity **(G)** and HOX genes **(F)** in NMP-derived trunk NC cultures treated with the indicated combinations of WNT-BMP agonists/antagonists.

Gogolou et al_Figure 4

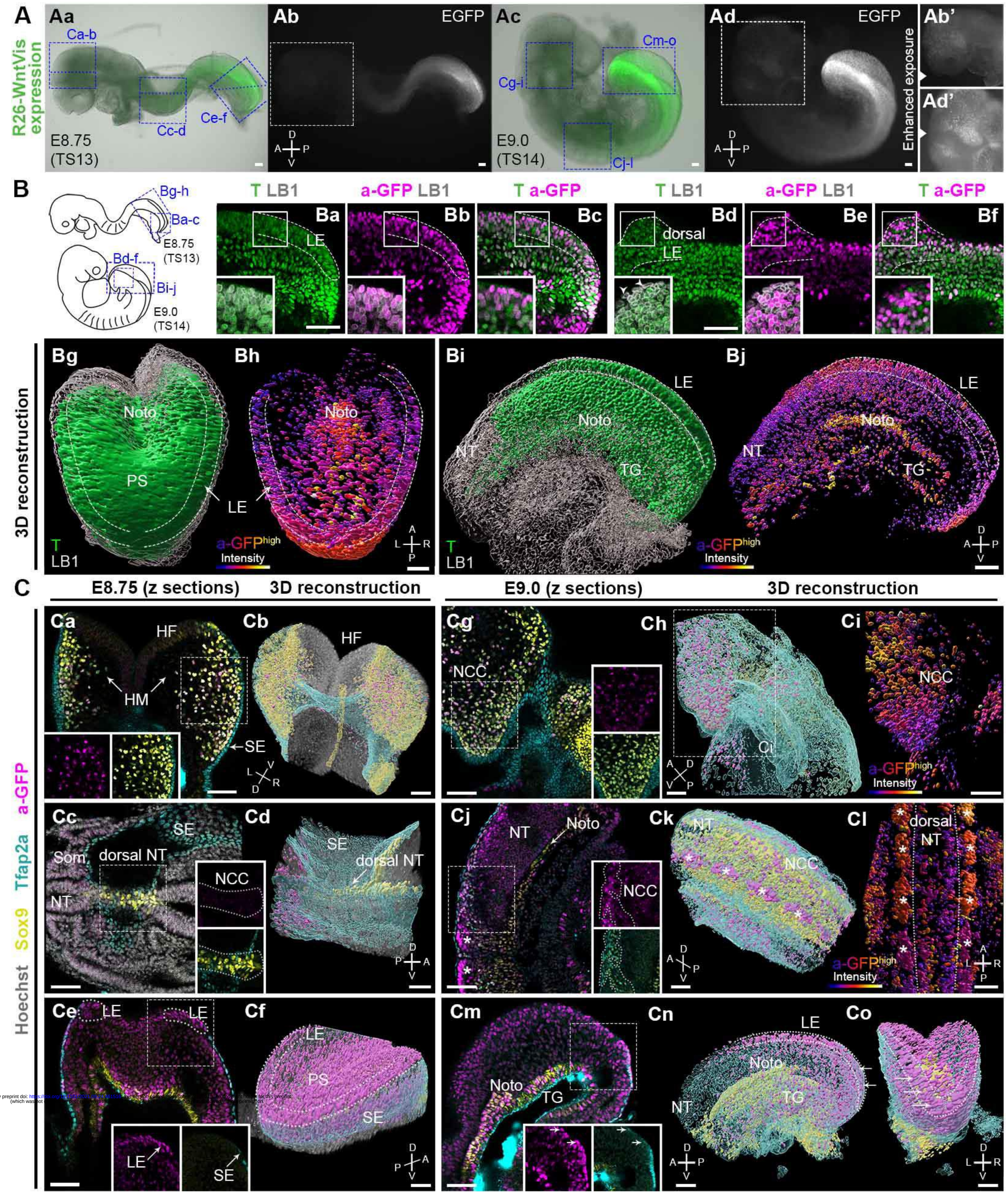

Figure 4. Wnt signalling dynamics during posterior neural crest emergence. (A) Fluorescence microscopy analysis of R26-WntVis mouse embryos at E8.75 (Theiler Stage; TS13) and E9.0 (TS14) showing graded responsiveness to WNT signalling in the posterior growth region. **(B)** Sagittal sections of immunostained R26-WntVis tail buds showing a-GFP signal in the T^+ lateral-most caudal epiblast (LE; dashed lines) at E8.75 (**Ba-c**) and E9.0 (**Bd-f**). **(Bg-j)** 3D reconstruction and processing of imaging data showing T^+ volumes overlapping with a-GFPhigh volumes (i.e. Wnt^{high} T^+ cells) in the LE: posterior view at E8.75 (**Bg-h**) and E9.0 (**Bi-j**). A cut-off was made to show only higher expressing a-GFP+ volumes (see **EV2**). Nuclei were defined by anti-Laminin B1 staining (LB1). **(C)** Wholemount immunostaining and corresponding 3D analysis showing NC derivatives and their progenitors at different sections of the rostrocaudal axis (regions corresponding to blue boxes in A). Insets corresponding to the dash line-boxed areas show the a-GFP and overlaid Sox9 and Tfap2a channels, respectively. (**Ca-b**, **Cg-i**) $Sox9^+$ $Tfap2a^+$ cells in the developing head mesenchyme. $Sox9^+$ $Tfap2a^+$ NC cells emerging from the E8.75 dorsal neural tube show low Wnt activity (**Cc-d**), whereas those at E9.0 generally exhibit a higher GFP signal (compare **Cc** to **Cj**). Asterisks mark dorsal somite cells. At E8.75, no $Tfap2a^+GFP^+$ cells were observed in the LE layer ($^{Ce-f}$), whereas at E9.0 the caudalmost epiblast contains a population of $Tfap2a^+$ GFP^+ cells (arrows in **Cm-o**). HF, headfolds; HM, head mesenchyme; NCC, neural crest cells; Noto, notochord; NT, neural tube; PS, primitive streak; Som, somite; SE, surface ectoderm; TG, tail gut; A, anterior; P, posterior; D, dorsal; V, ventral; L, left; R, right. Scale bars=50 μm.

Gogolou et al_Figure 5

A

Motif	Factor	P-value
	BRACHYURY	1e-615
	EOMES	1e-305
	TBX6	1e-295
	CDX4	1e-99
	LEF1	1e-84
	TCF3	1e-80
	CDX2	1e-79

B

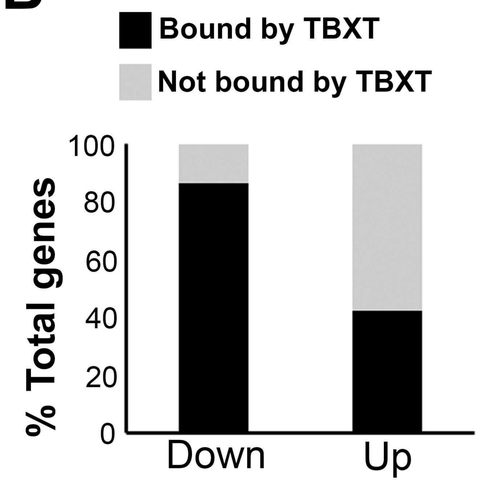

C

TBXT-bound (Distance from TSS=-1000 to 0 bp) genes affected by TBXT KD

DOWNREGULATED	UPREGULATED
MSGN1, **WISP1**, **HOXD3**, UNC5C, **TBX6**, **SNAI2**, **FOXF1**, FLJ12825, **DLL3**, **HOXA-AS3**, APLNR, TCERG1L, **HOXC5**, **FGF9**, PDGFRA, ARHGAP10, MYOF, **HOXA2**, HAS2, **MSX1**, MEIS2, CHST2, HHIPL2 SERPINE2, SLITRK5, RHBDF1, MLLT3, CDH24, LINC00458, **HOXB5**, RAB27A **TBXT**, RASL11B, GALNT10, PLEKHG3, AJUBA, PER1, NID2, UQCR11, KHDRBS3, **CDX1**, SDC2, HMGB2, **HOXA1**, ADGRL2 **DUSP7**, **WNT5B**, TLE3, RAP2B, **SP8**, **AXIN2** AKAP12, STAG1, AP1S2	RBL1, WDFY3, LRIG1, **JAG2**, TOX3, UTRN PCDH18, DAB1, PCDH1

NMP/PSM
HOX
NC/mesoderm
WNT
NOTCH
FGF

D

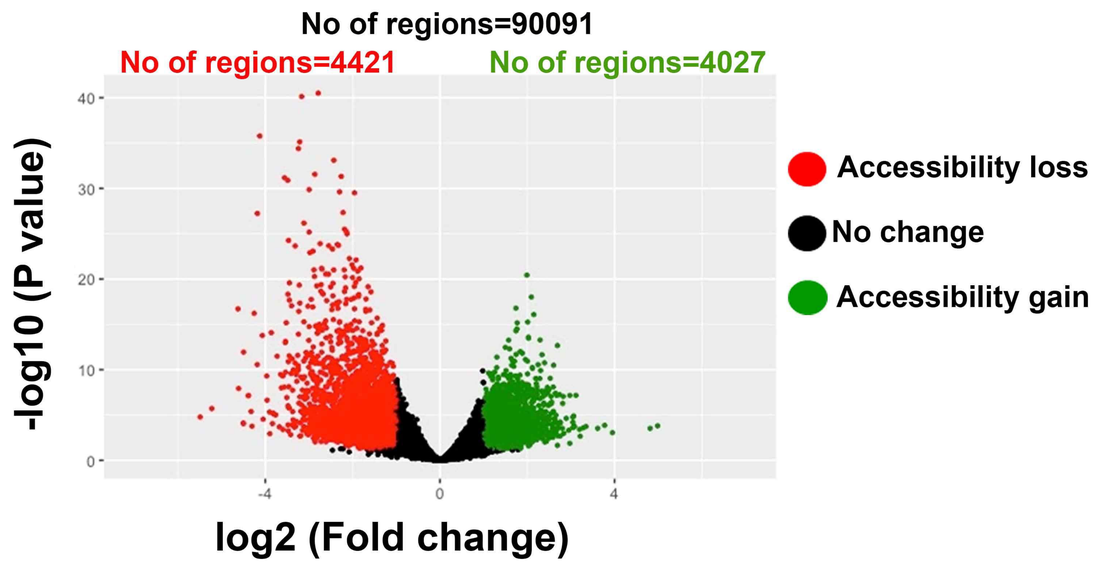

E

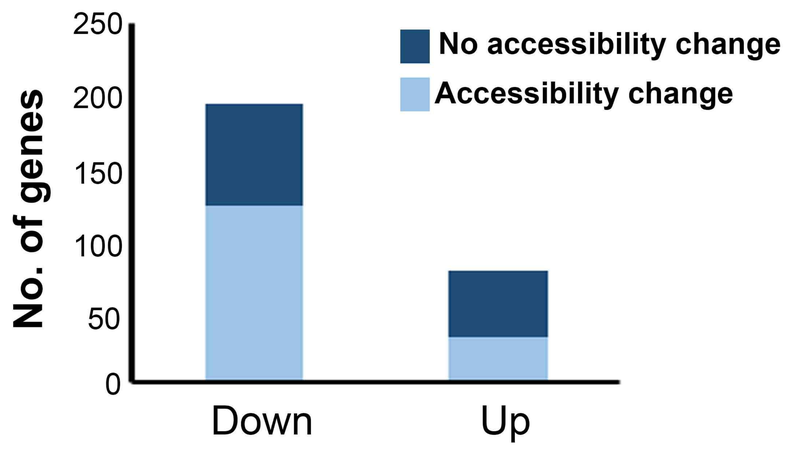

F

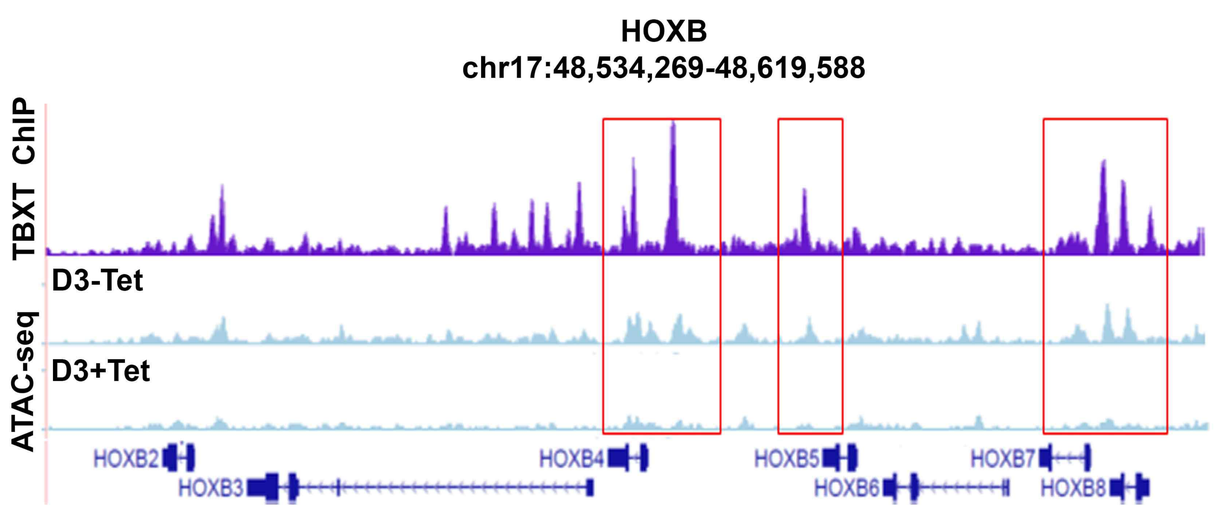

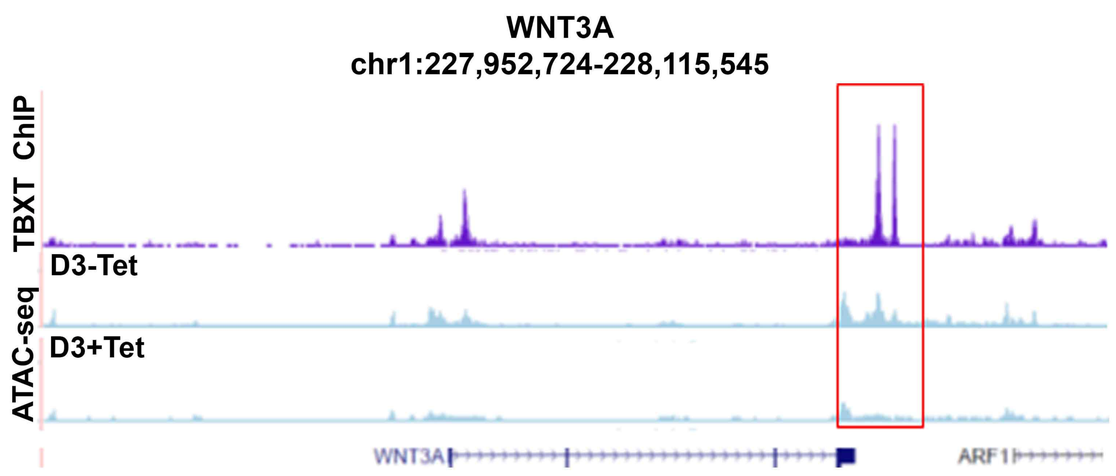

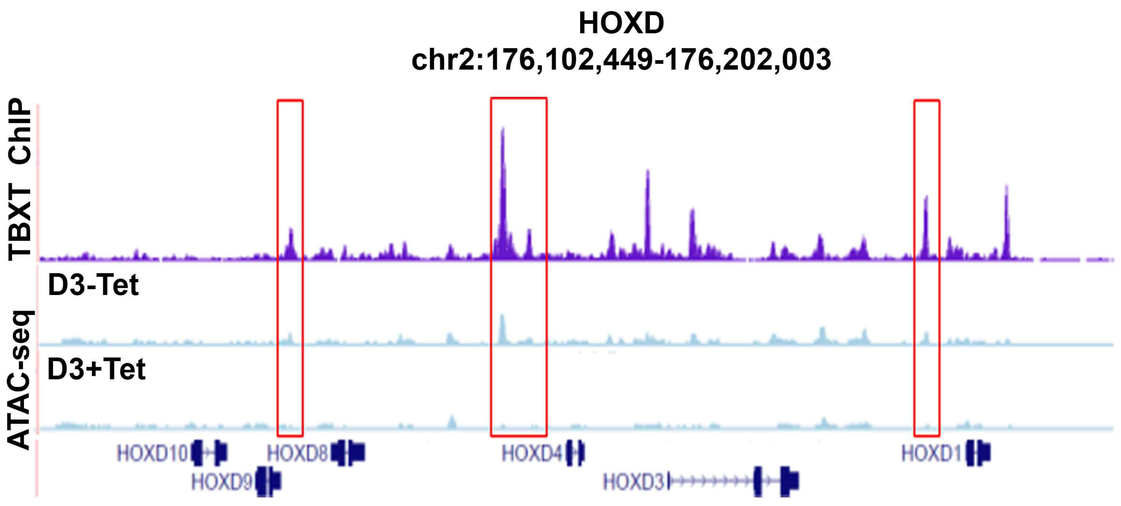

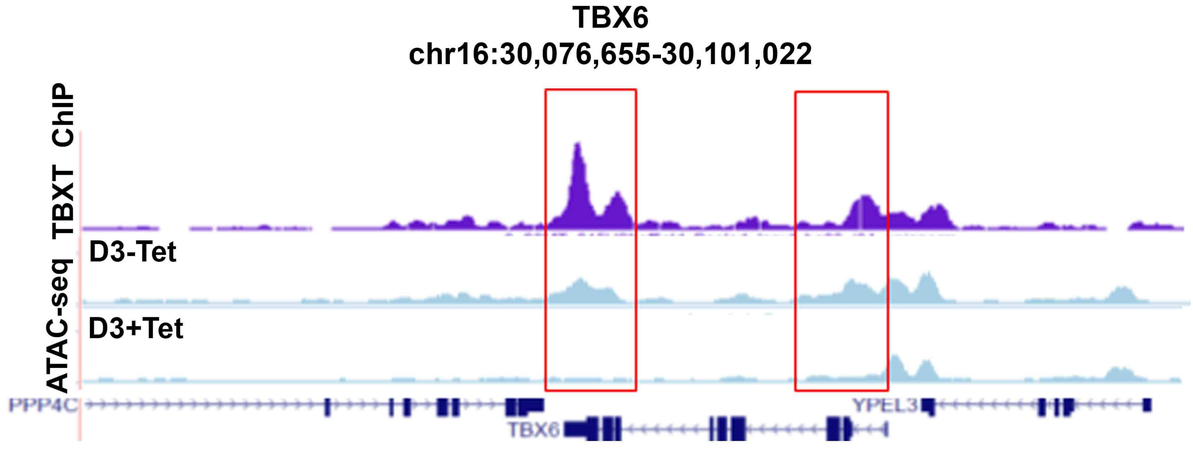

G

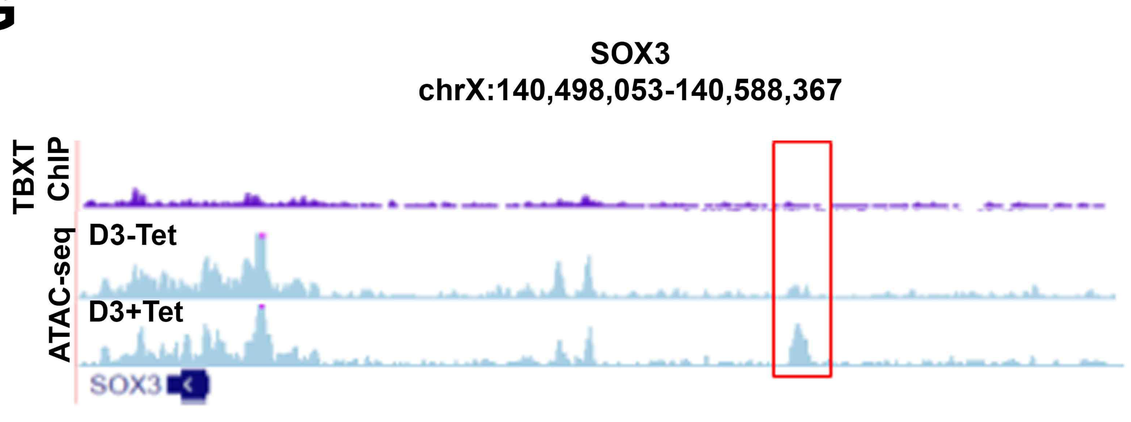

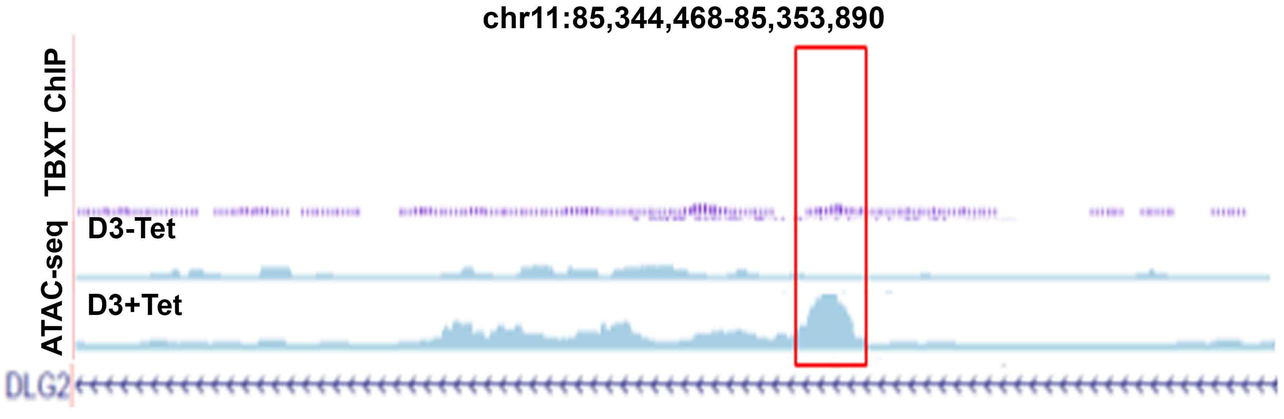

Figure 5. TBXT controls the HOX clock and WNT signalling in NMPs by influencing chromatin accessibility. (A) Representative transcription factor-binding motifs enriched in TBXT binding sites. **(B)** Graph showing the percentages of differentially expressed genes (Padj<0.05, log2FC> |1|) following TBXT knockdown during the transition of hESCs toward NMPs that are bound directly by TBXT. **(C)** Table showing all differentially expressed genes following TBXT knockdown that exhibit TBXT binding within their promoter region. **(D)** Volcano plot of differentially accessible ATAC seq peaks between TBXT-depleted and control NMPs. **(E)** Graph showing the number of significantly up- and down-regulated direct TBXT targets in relation to changes in chromatin accessibility associated with TBXT knockdown. **(F)** Correspondence between TBXT binding (ChiP) and chromatin accessibility changes (ATAC-seq) in the presence and absence of Tet in indicated HOX clusters, WNT/presomitic mesoderm-linked loci. **(G)** Correspondence between TBXT binding and chromatin accessibility changes in the presence and absence of Tet in indicated neural differentiation-linked loci.

Gogolou et al_Figure 6

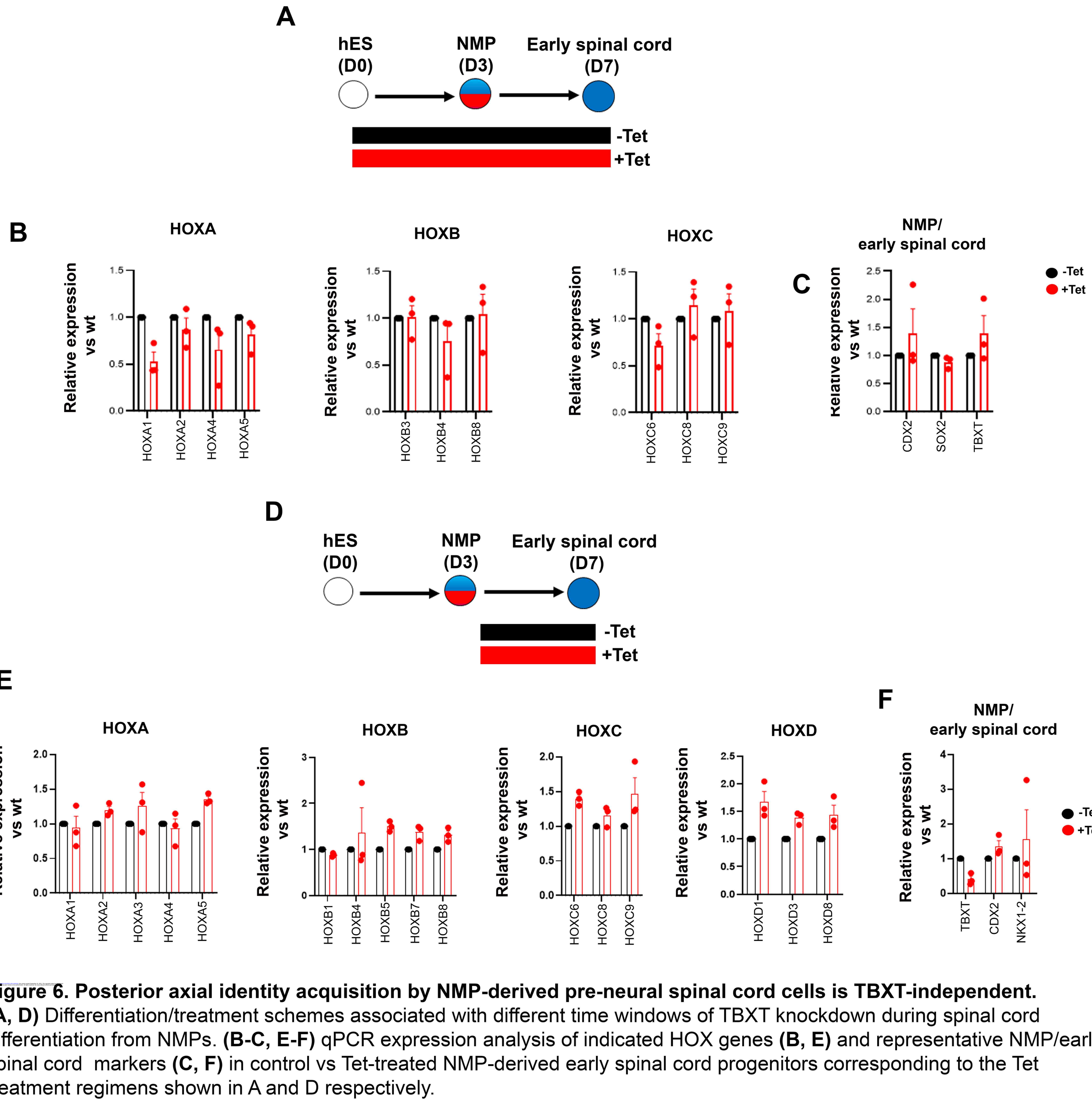

Figure 6. Posterior axial identity acquisition by NMP-derived pre-neural spinal cord cells is TBXT-independent.
(A, D) Differentiation/treatment schemes associated with different time windows of TBXT knockdown during spinal cord differentiation from NMPs. **(B-C, E-F)** qPCR expression analysis of indicated HOX genes **(B, E)** and representative NMP/early spinal cord markers **(C, F)** in control vs Tet-treated NMP-derived early spinal cord progenitors corresponding to the Tet treatment regimens shown in A and D respectively.

Gogolou et al_Figure 7

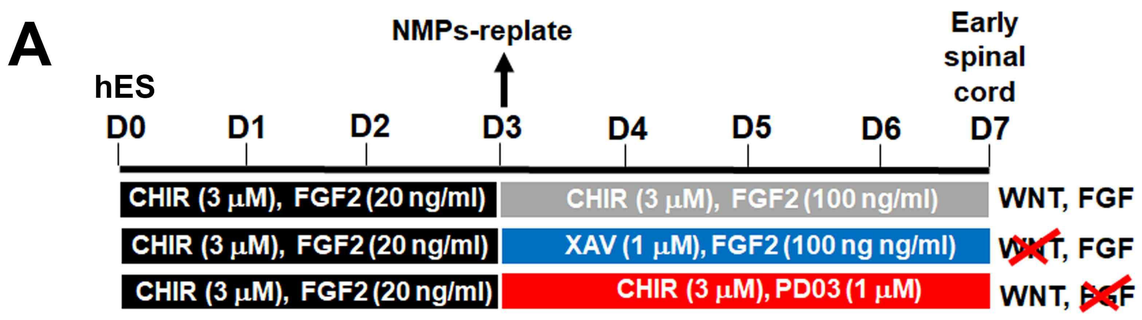

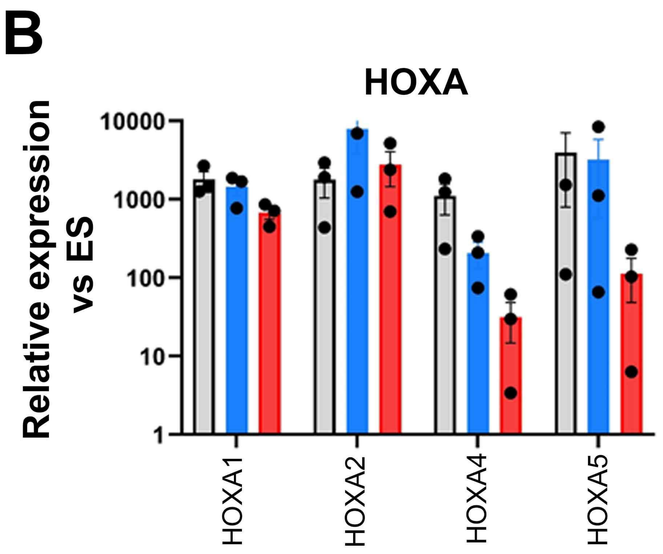

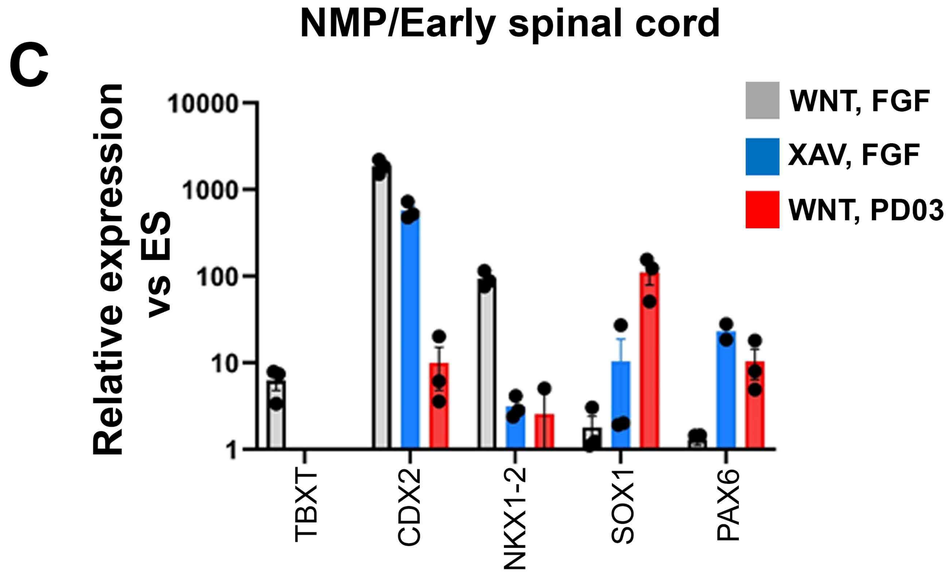

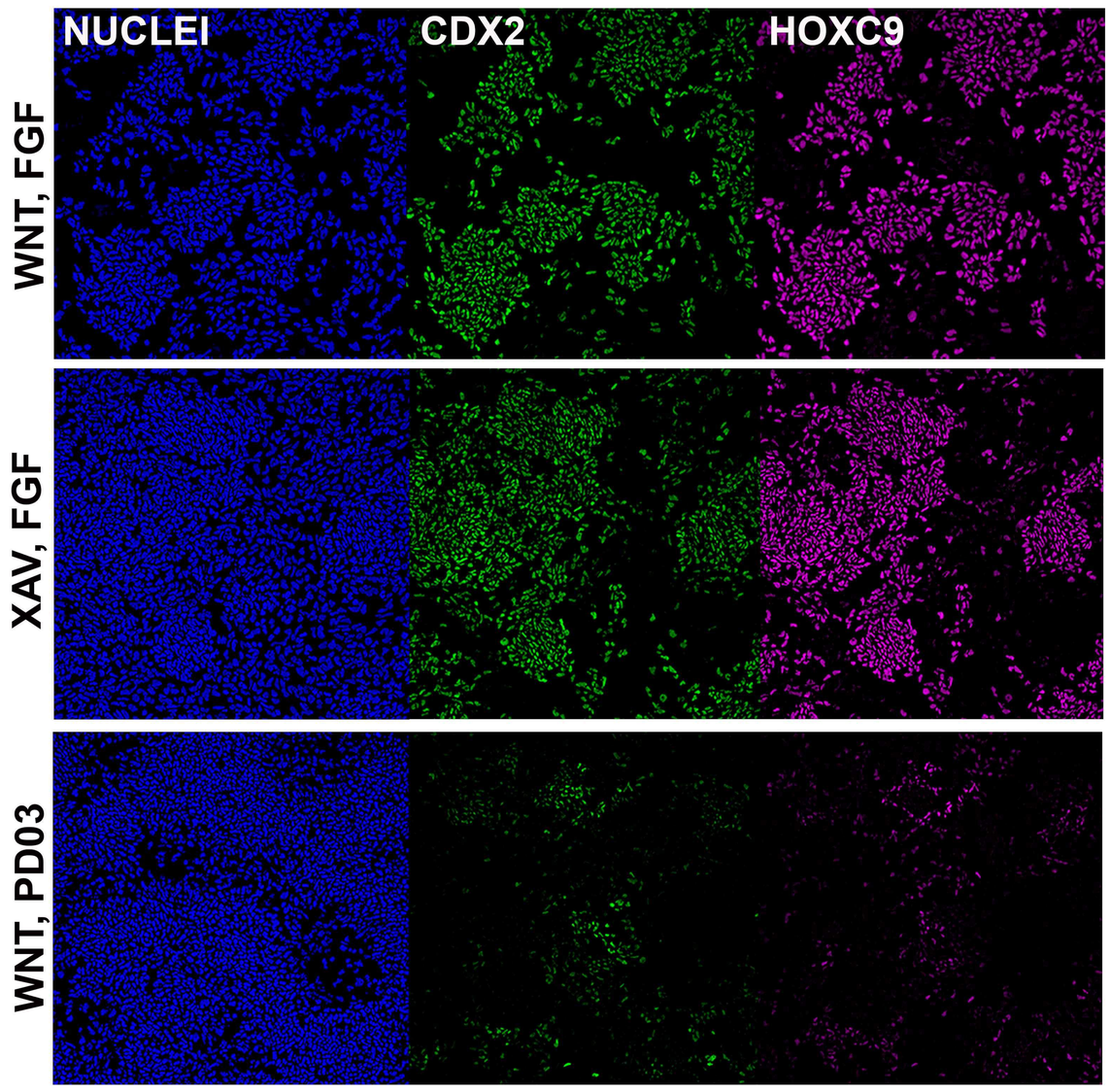

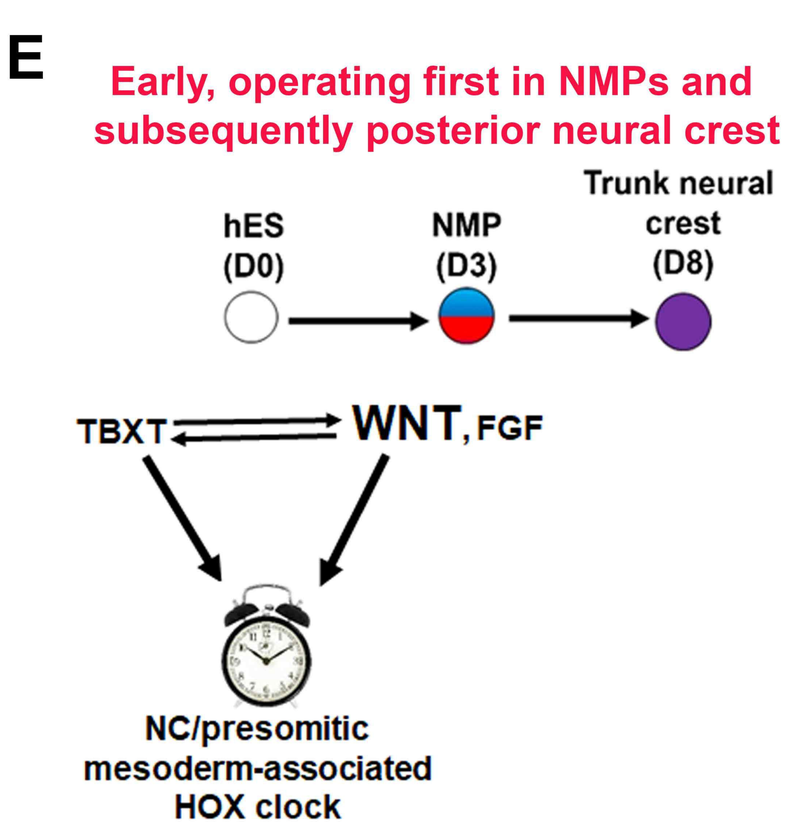

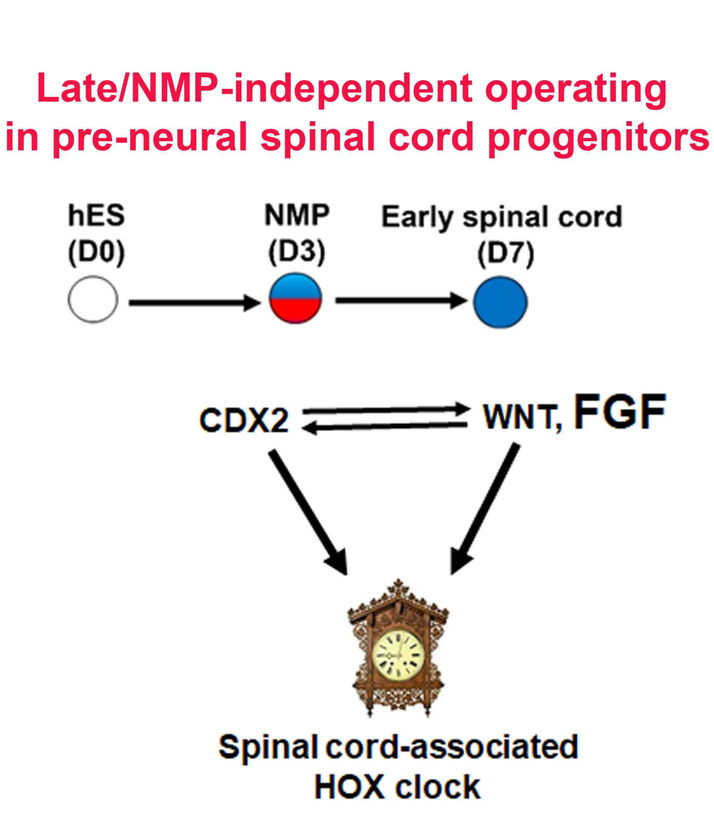

Figure 7. Posterior axial identity acquisition by NMP-derived spinal cord progenitors is FGF-dependent. (A) Scheme of treatments during the differentiation of hPSC-derived NMPs toward early spinal cord progenitors. **(B-C)** qPCR expression analysis of indicated HOX genes **(B)** and representative NMP/early spinal cord/neural markers **(C)** in NMP-derived early spinal cord cultures treated with the indicated combinations of WNT-FGFagonists/antagonists as depicted in A. **(D)** Immunofluorescence analysis of CDX2 and HOXC9 protein expression in NMP-derived early spinal cord cultures treated with the indicated combinations of WNT-FGF agonists/antagonists. **(E)** Proposed model for the transcriptional and signalling control of posterior axial identity/Hox clock in hPSC-derived NMPs and their derivatives.